Environmental Science: Atmospheres

ROYAL SOCIETY OF CHEMISTRY

PAPER

View Article Online
View Journal | View Issue

Cite this: *Environ. Sci.: Atmos.*, 2024, **4**, 1413

URMELL – part II: semi-explicit isoprene and aromatics gasSOA modelling†

Marie Luise Luttkus, *[a] Erik Hans Hoffmann, [b] Andreas Tilgner, [b] Jana Wackermann,[a] Hartmut Herrmann [b] and Ralf Wolke [a]

Oxidation of emitted anthropogenic and biogenic volatile organic compounds (VOCs) and subsequent chemical reactions reduce the volatility of the products formed leading to secondary organic aerosol (SOA) formation. Despite the huge diversity of individual SOA compounds, SOA modelling is often simplified and estimated at the initial oxidation step neglecting chemical and physical process influencing SOA formation *e.g.* advection, deposition, chemical degradation and aging processes. To overcome this shortcoming, the chemical gas-phase mechanism URMELL was developed. URMELL treats more than 40 distinct oxidised gas-phase SOA (gasSOA) precursors with individual molecular characteristics and physico-chemical partitioning properties enabling a much more explicit gasSOA treatment for products of aromatics and isoprene oxidation. In this study, CTM simulations using COSMO-MUSCAT were performed with URMELL and compared with a simplified gasSOA scheme applying the widely used gas-phase mechanism RACM. The comparison indicates a delayed and thereby locally shifted gasSOA formation when applying URMELL. This effect is caused by the formation of multigenerational and multifunctional products along the transport trajectory whereby accounting for changes in the oxidant regime and leading to a multitude of gasSOA substances with URMELL. For isoprene and aromatics, URMELL simulates higher contributions of products with lower volatilities whereby aromatics generate even non-volatile products which can partition in new particle formation. The non-volatile aromatic products increase the average aromatic surface gasSOA concentration (30% on 20th of May 2014) and show unexpectedly high concentrations in remote spruce forest areas, away from the emission sources, highlighting the potential of the detailed schemes and its need for application in CTMs.

Received 3rd June 2024
Accepted 21st October 2024

DOI: 10.1039/d4ea00075g

rsc.li/esatmospheres

Environmental significance

The oxidation of anthropogenic and biogenic volatile organic compounds (VOCs) leads to the formation of low volatile products which can partition into the particle-phase through condensation processes contributing to particle mass formation. Depending on the atmospheric oxidation regime, independent SOA pathways emerge. Such differences can be missed using the classical, but simplified, VBS or 2p approach. Therefore, an explicit SOA scheme for aromatics and isoprene has been developed and coupled to the gas-phase mechanism URMELL. Adjunct model simulations for Germany highlight the effect of the interplay between VOC advection and their chemical degradation resulting into SOA formation far from emission sources, especially for aromatic compounds. The study highlights the efficiency of the detailed scheme and its need for application in chemical transport models.

1. Introduction

Secondary Organic Aerosol (SOA) is a crucial mass fraction of aerosol particles, which impact air quality, human health and climate.[1–3] SOA is produced by oxidation of non-methane volatile organic compounds (NMVOCs) which can be of anthropogenic (AVOC) or biogenic (BVOC) origin.[4,5] However, the majority of NMVOCs are BVOCs emitted from vegetation.[3,6,7] Subsequent chemical degradation of NMVOCs results in less volatile oxidation products that can condense onto existing aerosol particles and/or facilitate new particle formation. This is governed *e.g.* by atmospheric oxidative and photochemical conditions (*e.g.* $NO_x = NO + NO_2$; $HO_x = OH + HO_2$; O_3), as well as meteorological parameters (radiation, temperature, humidity). All in all, NMVOC oxidation impacts particle growth, new particle formation as well as cloud and precipitation processes by affecting the chemical aerosol composition, aerosol particle number and size distribution.[8–14] Thus, SOA affects Earth's climate directly by absorption and scattering of incoming solar radiation or indirectly by contributing to cloud

[a]*Department Modelling of Atmospheric Processes, Leibniz Institute for Tropospheric Research (TROPOS), Permoserstr. 15, 04318 Leipzig, Germany. E-mail: luttkus@tropos.de*

[b]*Atmospheric Chemistry Department (ACD), Leibniz Institute for Tropospheric Research (TROPOS), Permoserstr. 15, 04318 Leipzig, Germany*

† Electronic supplementary information (ESI) available. See DOI: https://doi.org/10.1039/d4ea00075g

formation and precipitation.[3,15–18] *Vice versa*, a change in the radiation budget and precipitation impacts the oxidation capacity of the atmosphere and effects dry and wet deposition feeding back into SOA formation processes.[19–25]

During daytime conditions, NMVOC oxidation is dominated by reaction with OH radicals and O_3, while during the night, the dominant oxidant is the NO_3 radical.[6,23,26–28] Due to the high variety of NMVOCs emitted and their individual degradation pathways driven by environmental conditions, a huge diversity of SOA precursors exists. Recent studies revealed a high impact of SOA formation through NMVOC oxidation from the NO_x concentration.[14,23,27,29–31] For isoprene, high NO concentrations lower, while high NO_2 concentrations increase the gasSOA yield in comparison to no NO_x conditions.[31–34] Linking anthropogenic and biogenic NMVOC degradation processes under varying environmental conditions including NO_x dependencies creates complex NO_x–O_3–SOA interlinkages relevant for air quality and climate.[3,14,28,35–37] Thus, it is of utmost importance to account for these complex interdependencies in chemical transport (CTMs) and earth system models (ESMs).

It was revealed recently, that the model representation of BVOC emissions, their oxidation, SOA formation and particle size distribution dynamics are crucial sources for the still relatively high uncertainty of the aerosol–cloud–climate feedbacks as presented in the IPCC.[35,38–40] Globally, isoprene is the most abundant BVOC, followed by monoterpenes and sesquiterpenes.[7] Nevertheless, in terms of SOA formation, sesquiterpenes followed by monoterpenes and isoprene have the highest potentials.[41–43] Therefore, isoprene dominates the SOA composition in isoprene-dominated regions such as the tropical rain forests, but on a regional scale, especially in coniferous forests, the oxidation of monoterpenes mainly drives SOA formation.[9,28,44–46] The contribution of sesquiterpenes to the overall SOA budget is assumed to be low, due to their lower emission rates, but even little contributions can enhance SOA production *via* the formation of ultralow-volatile organic compounds from RO_2 cross reactions.[41] Such dependencies demonstrate a strong linkage between BVOC emissions and biogenic SOA (BSOA) formation which have to be represented in models adequately. Thus, factors controlling BVOC emissions such as taxonomic biodiversity, meteorological drivers (*e.g.* temperature and radiation) and stressors (*e.g.* heat, drought or herbivore infestation) impact SOA formation modelling.[7,28,47–52]

In addition, within urban and industrial areas AVOCs are of high importance of which aromatics, higher alkenes and alkanes being the most important anthropogenic SOA (ASOA) precursors.[3,28,42,53] Major AVOC sources are the transport sector, industry and biomass burning. Global simulated AVOC SOA burden is about 40%, but the contribution between BVOCs and AVOCs differs significantly in space and time.[3,28,42,54] Moreover, BVOC and AVOC emissions as well as their SOA contributions are likely to change due to land use change, climate warming and adaptation as well as air quality measures which further complicates adequate air quality and climate assessments and predictions.

Even though there is a huge variety of NMVOCs, current chemical mechanisms applied in CTMs include only a few mainly lumped species.[55–61] Still, an accurate description of the chemical formation and decomposition of SOA precursor substances within chemical mechanisms used in CTMs is crucial for an adequate air quality assessment. This includes the treatment of diverse AVOC and BVOC sources. Often, SOA precursors are partly lumped into the following NMVOC clusters: xylene, toluene, cresols, isoprene, monoterpenes, sesquiterpenes, higher alkanes and alkenes. However, the SOA forming potential of an individual species within such a lumped NMVOC cluster can vary significantly.[8,62–67]

In addition to the uncertainties discussed above, SOA formation within CTMs/ESMs has mainly been described using a two product (2p) or volatility basis set (VBS) approach which often lumps all considered SOA products into 5 volatility bins.[28–30,42,68–72] These approaches determine the SOA forming potential of all parent NMVOCs considered at the first oxidation step based on a few hypothetical products with certain empirical gas/particle partitioning parameters. Some of these also include a NO_x dependency for OH radical initiated SOA concentrations.[29,30,73] But, a simple NO_x dependency can lead to an over or under prediction of the simulated SOA mass concentration as NO and NO_2 can have opposing effects.[14,31–34] However, most SOA products form through multiple subsequent chemical reaction chains leading to a variety of different low to non-volatile products with individual properties. To account for multigenerational products simplified unconstrained aging parameterisations are applied to 2p/VBS schemes shifting a semi-volatile product into the next lower volatility bin/class.[42,71,73,74]

But still, the use of a classical 2p or VBS decouples SOA formation from the actual/real chemical processes. Transport-related induced changes in environmental conditions including a switch from polluted to clean environments or the integration of additional pathways such as the formation of stable accretion products (ROOR or dimers) from the reaction of two RO_2 radicals[41,75–81] are not represented sufficiently enough by current SOA approaches. Furthermore, these simplified schemes do not differentiate between SOA formed from the gas- (gasSOA) and the aqueous- (aqSOA) or particle-phase.[82–85] Depending on the experimental conditions at which the SOA yield parameters for the simplified 2p/VBS SOA approach were determined from it can include aqSOA. For isoprene, Stadtler *et al.*[86] applied a more detailed SOA scheme considering four gasSOA and two aqSOA products in the ESM ECHAM-HAMMOZ and compared it to a classical VBS approach. The comparison revealed the production of non-volatile and aqSOA products, which are both not considered in the classical VBS approach, in addition to the low- and semi-volatile products which favour the production of more volatile products.

Within ECHAM-HAMMOZ, the Jülich Atmospheric Mechanism (JAM) is implemented. For the previous mentioned study[86] a slightly revised variation of JAM version 2 (ref. 57) was used. JAM version 2 was also the basis for the gas-phase mechanism URMELL[19] (short for Urban and Remote cheMistry modELLing), but URMELL includes substantial updates as it comprises sophisticated isoprene and aromatic chemistry schemes and a variety of individual SOA products (26 aromatic- and 20

isoprene-related gasSOA species). Thus, URMELL enables an explicit and direct gasSOA approach by maintaining highly-oxidised reaction products. URMELL allows for the consideration of transport-related changes in the $O_3/HO_x/NO_x$ regime and investigations on how this impacts the products formed and their physico-chemical characteristics. Thus, applying URMELL helps to gain improved knowledge in the underlying chemical processes and to estimate the detail needed to adequately describe gasSOA formation. In this study, the semi-explicit gasSOA modelling approach of URMELL is applied and compared to a 2p approach using the CTM COSMO-MUSCAT and the differences are discussed. Finally, conclusions and implications of this study are presented.

2. Semi-explicit gasSOA modelling approach

In general, common gasSOA estimates are based on a so-called 2-product (2p) or VBS SOA approach. Both these approaches determine gasSOA based on fixed, empirically derived partitioning parameters (*e.g.* $p_i^*/C_{sat,i}^*$) for a subset of hypothetical products at the initial oxidation step for all considered parent NMVOCs.[28–30,68–72] The oxidation of VOCs is described within the applied gas-phase chemical mechanism, in this study RACM[55] and URMELL[19] are used. VOC oxidation is mainly initialised by a reaction with OH, O_3 or NO_3 and produce numerous reaction products of which some maybe semi-volatile and able to partition between the gas and particle phase. Progressing chemical degradation of VOCs creates organic products characterized with a multitude of chemical functionalities resulting into lower volatility. The lower volatility enables an enhanced partitioning towards the particle phase. Therefore, a fraction of the semi-volatile reaction products will transfer into the particle-phase which is of particular interest for SOA concentration estimation. In 1994, Pankow[5] introduced an absorption model describing the gas/particle partitioning appropriable for organic compounds including such semi-volatile reaction products.

In COSMO-MUSCAT (see Section 3 for details), SOA formation follows the recommendations by Schell *et al.*,[68] which are based on the Pankow approach.[5] Following Schell *et al.*,[68] the total concentration $C_{tot,i}$ (μg m^{-3}) of a certain semi-volatile reaction product i is the sum of its gas- $C_{gas,i}$ (μg m^{-3}) and particle-phase $C_{part,i}$ (μg m^{-3}) concentration:

$$C_{tot,i} = C_{gas,i} + C_{part,i}. \quad (1)$$

Assuming a quasi-ideal solution and following Raoult's law the partial pressure p_i (Pa) of an individual compound i in the gas phase above the particle is the product of its mole fraction $\chi_{i,om}$ in the solution and its saturation vapour pressure as a pure liquid p_i^*. In combination with the ideal gas law the gas-phase saturation concentration $C_{sat,i}$ (μg m^{-3}) is as given by Schell *et al.*:[68]

$$C_{sat,i} = \chi_{i,om} \times \frac{p_i^* \times m_i \times 10^6}{R \times T} = \chi_{i,om} \times C_{sat,i}^*, \quad (2)$$

where R is the gas constant (8.314 J mol^{-1} K^{-1}), T the temperature (K), m_i the molar mass of compound i and $C_{sat,i}^*$ (μg m^{-3}) the saturation concentration as pure liquid compound. The mole fraction is calculated as follows (Schell *et al.*[68]):

$$\chi_{i,om} = \frac{\frac{C_{part,i}}{m_i}}{\sum_{j=i}^{n}\left(\frac{C_{part,j}}{m_j}\right) + \frac{C_{ini}}{m_{ini}}}, \quad (3)$$

where C_{ini} is the concentration of any additional absorbing organic material, m_j and m_{ini} are the molar masses.[68]

Within COSMO-MUSCAT the p_i^* notation is directly used instead of the typical use of $C_{sat,i}^*$ within the VBS approach. The aerosol mass concentration is calculated as follows and can be derived from the equations provided by Schell *et al.*:[68]

$$C_{part,i} = \frac{C_{tot,i}}{1 + \frac{p_i^* \times 10^6}{R \times T} \times \frac{1}{\sum_{j=i}^{n}\left(\frac{C_{part,j}}{m_j}\right) + \frac{C_{ini}}{m_{ini}}}}, \quad (4)$$

where C_{ini} is the concentration of any additional absorbing organic material, m_j and m_{ini} are the molar masses. While $C_{tot,i}$ is calculated through the chemical mechanism, the calculation of $C_{part,i}$ creates a set of n nonlinear equations which have to be solved *via* iteration. In COSMO-MUSCAT, this is done by the Newton–Raphson method. For the pure compound vapour pressure p_i^*, the Clausius–Clapeyron equation is used to capture the temperature dependence:

$$p_i^* = p_i^{*R} \times \exp\left[-\frac{\Delta H_{vap}}{R} \times \left(\frac{1}{T} - \frac{1}{T^R}\right)\right], \quad (5)$$

with p_i^{*R} being the reference vapour pressure of compound i at the reference temperature T^R (298 K) and the enthalpy of vaporisation ΔH_{vap} (J mol^{-1}).[68] Note that based on (eqn (4)), the portion of a certain SOA precursor substance in the particle-phase increases with increasing total absorbing organic matter.

While for the 2p or VBS SOA approaches fixed partitioning parameter values (*e.g.* $p_i^*/C_{sat,i}^*$, ΔH_{vap}) at a certain reference temperature are used for a subset of hypothetical products, the knowledge of a multitude of real, distinct SOA products allows for structural based temperature dependent estimates of these parameters. Therefore, an explicit SOA approach enables the determination of p_i^* and ΔH_{vap} for varying temperatures based on their chemical structure. Estimating p_i^* is a crucial task for SOA formation parameterisations, however, it is associated with a high level of uncertainty. Different methods can be used to determine p_i^* based on chemical structures. Pending on the method used, deviations of up to three orders of magnitude can be reached. In this study, p_i^* estimates based on the molecular structure from several online frameworks: the Generator for Explicit Chemistry and Kinetics of Organics in the Atmosphere GECKO-A,[87] EVAPORATION[88,89] and UManSysProp[90,91] are used. GECKO-A provides several parameters based on the molecular structure (molar weight, boiling point estimates, hydration constants, effective Henry's law constant) including p_i^* values for three different methods at 298 K. The three methods are: (i)

Myrdal and Yalkowsky[92] with boiling points from the Joback group contribution method;[93,94] (ii) Nannoolal[95] with boiling points from the Nannoolal contribution method[96,97] and (iii) SIMPOL-1 (ref. 98). Additionally, (iv) the EVAPORATION method[88] is used. To estimate temperature-dependent p_i^* values for method (i) and (ii) the online tool UManSysProp is used. For URMELL, the lowest value established with these four methods is applied where feasible to reach for the upper limit. Compared to the 2p or VBS approach which use empirical estimates for hypothetical SOA substances, the knowledge of the individual molecular structures provides the opportunity to estimate p_i^* values for varying temperatures using the four methods. Based on the molecular structures of the explicit URMELL SOA species, p_i^* values for: 268 K, 273 K, 278 K, 283 K, 288 K, 293 K and 298 K are calculated. Furthermore, this enables the determination of a temperature-dependent equation for ΔH_{vap}. The conversion of eqn (4) gives:

$$\Delta H_{vap} = \frac{R \times \ln\left(\frac{p_i^{*R}}{p_i^*}\right)}{\left(\frac{1}{T} - \frac{1}{T^R}\right)}. \quad (6)$$

Here, p_i^{*R} is set to the reference temperature of 298 K. Plotting this into a simple x–y diagram and interpolating provides a linear fit function of the type:

$$\Delta H_{vap}(T) = a \times T + b, \quad (7)$$

where a is the slope and b is the y-intercept. As an example, the plot for the compound DHHPEPOX is provided in the ESI (Fig. S1-1)† including the linear fit function. This method was applied to all explicit SOA species and the calculated values are provided in Sections 2.1–2.3. For cases where the 2p approach is installed, a is set to 0 and $\Delta H_{vap}(T)$ becomes a constant again. Tables 1–3 summarize all parameters (molecular weight MW in g mol^{-1}, p_i^{*R} in Pa for 298 K, slope a, y-intercept b) necessary for the explicit SOA parameterisation with URMELL using COSMO-MUSCAT. Tables 1–3 also contain the URMELL species name and the corresponding notation for the particle-phase, where the abbreviation CP stands for concentration in the particle-phase.

2.1. Explicit gasSOA through phase partitioning of aromatic oxidation products

To enable explicit gasSOA formation, the aromatic chemistry was extended and resulting on the molecular structure based p_i^* estimates 26 gasSOA precursor compounds (see Table 1) including organic nitrates (BENZN, TOLN, XYLNO3, NPHENOLOOH, NCRESOOH), nitro-phenols (NPHEN, N2PHEN, NPHENOOH, NCATECHOL), furanones (BZFUONEOOH, FUONEOOH), quinones (BZQOOH, BZQCO, NBZQOOH) and maleic anhydride (MALANHYOOH) had been included in URMELL.[19] Furthermore, a non-volatile multigenerational end product is considered (NAROMOLOOH) lumping two peroxide-bicyclic alkenes with five functional groups whereby the

Table 1 Aromatic gasSOA species notation within the URMELL gas-phase mechanism and SOA module, the molecular weight (MW), reference saturation vapour pressure (p_i^{*R}) and parameter a and b for calculating the temperature-dependent enthalpy of vaporisation. The species NAROMOLOOH is treated as non-volatile, here the values for NCATECHOOH are given

URMELL species	SOA notation	MW (g mol^{-1})	p_i^{*R} (Pa)	a (kJ mol^{-1} K^{-1})	b (kJ mol^{-1})	Method
BENZOOH	CPBENZOOH	160.14	1.36×10^{-2}	−87.973	121 933	iv
BENZN	CPBENZN	189.14	9.95×10^{-2}	−85.4	116 571	iv
BENZ=O	CPBENZ=O	142.12	1.65×10^{0}	−68.2	92 447	iv
BZFUONEOOH	CPBZFUONEOOH	134.1	1.5×10^{-3}	−140.72	144 120	ii
C5DIALOOH	CPC5DIALOOH	130.11	1.18×10^{0}	−70.1	94 280	iv
NPHENOLOOH	CPNPHENOLOOH	221.14	3.18×10^{-4}	−107.96	146 787	iv
PHENOOH	CPPHENOOH	176.14	1.11×10^{-4}	−48.058	118 127	i
NPHEN	CPNPHEN	139.12	3.33×10^{-2}	−46.963	98 343	i
N2PHEN	CPN2PHEN	184.12	4.39×10^{-6}	−47.511	126 521	i
NPHENOOH	CPNPHENOOH	155.12	1.66×10^{-3}	−48.058	108 615	i
CATEC1OOH	CPCATEC1OOH	126.12	1.31×10^{-1}	−98.388	112 971	ii
NCATECHOL	CPNCATECHOL	155.12	1.99×10^{-4}	−46.963	115 249	i
NAROMOLOOH	CPNAROMOLOOH	300.0	1.0×10^{-10}	−48.606	136 373	i
MALANHYOOH	CPMALANHYOOH	148.08	1.18×10^{-3}	−101.39	139 990	iv
BZQOOH	CPBZQOOH	158.12	3.17×10^{-5}	−47.511	121 369	i
BZQCO	CPBZQCO	140.1	1.37×10^{-3}	−46.963	108 600	i
NBZQOOH	CPNBZQOOH	203.12	1.91×10^{-5}	−49.154	123 150	i
TOLOOH	CPTOLOOH	174.17	1.01×10^{-2}	−48.058	103 265	i
TOLN	CPTOLN	203.17	5.15×10^{-2}	−89.82	120 808	iv
TOL=O	CPTOL=O	156.15	8.54×10^{-1}	−70.72	96 173	iv
CRESOOH	CPCRESOOH	150.15	3.15×10^{-5}	−48.058	121 860	i
NCRESOOH	CPNCRESOOH	235.17	1.65×10^{-4}	−111.16	150 698	iv
FUONEOOH	CPFUONEOOH	148.13	1.13×10^{-3}	−143.16	146 317	ii
C615CO2OOH	CPC615CO2OOH	144.14	3.85×10^{-1}	−74.68	100 342	iv
XYLENOOH	CPXYLENOOH	188.18	2.91×10^{-3}	−48.058	107 122	i
XYLN	CPXYLN	217.18	2.66×10^{-2}	−91.63	124 337	iv

Table 2 Isoprene gasSOA species notation in the URMELL gas-phase mechanism and SOA module, the molecular weight (MW), reference saturation vapour pressure (p_i^{*R}) and parameter *a* and *b* for calculating the temperature-dependent enthalpy of vaporisation

URMELL species	SOA species notation	MW (g mol^{-1})	p_i^{*R} (Pa)	*a* (kJ mol^{-1} K^{-1})	*b* (kJ mol^{-1})	Method
LHMVKABOOH	CPLHMVKABOOH	120.12	1.81×10^{-1}	−95.302	111 499	ii
MACR2NOOH	CPMACR2NOOH	181.12	5.23×10^{-3}	−123.36	138 027	ii
IHNEOOH	CPIHNEOOH	195.15	3.19×10^{-4}	−148.96	157 768	ii
MACRNOOH	CPMACRNOOH	165.12	1.08×10^{-1}	−99.02	115 789	ii
LHMVKNOOH	CPLHMVKNOOH	165.12	8.86×10^{-2}	−101.36	116 096	ii
MACROOH	CPMACROOH	120.12	7.09×10^{-2}	−102.35	118 910	ii
NISOPOOHOOH	CPNISOPOOHOOH	213.17	2.92×10^{-7}	−218.36	211 085	ii
NISOPOOHOH=O	CPNISOPOOHOH=O	195.15	1.93×10^{-4}	−153.49	161 504	ii
NISOPNOOH	CPNISOPNOOH	242.17	3.32×10^{-6}	−193.96	192 078	ii
NISOPOHOH=O	CPNISOPOHOH=O	179.15	5.01×10^{-4}	−51.346	115 321	i
LISOPNO3NO3=O	CPLISOPNO3NO3=O	224.15	2.47×10^{-4}	−52.99	117 907	i
LISOPNO3OOH	CPLISOPNO3OOH	197.17	3.26×10^{-6}	−193.73	192 257	ii
LISOPNO3NO3	CPLISOPNO3NO3	226.17	9.86×10^{-6}	−55.537	129 040	i
LISOPOOHOOH	CPLISOPOOHOOH	168.17	1.62×10^{-7}	−225.23	215 756	ii
LIECO3H	CPLIECO3H	148.13	2.90×10^{-3}	−4.6815	93 100	iii
LHC4ACCO2H	CPLHC4ACCO2H	116.13	4.76×10^{-2}	−82.568	113 540	iv
LC578OOH	CPLC578OOH	150.15	9.38×10^{-5}	−50.798	121 245	i
DHHPEPOX	CPDHHPEPOX	128.13	2.63×10^{-4}	−105.13	144 415	iv
DHPMEK	CPDHPMEK	136.12	8.82×10^{-3}	−121.39	132 233	ii
DHPMPAL	CPDHPMPAL	136.12	1.03×10^{-2}	−118.69	132 211	ii

Table 3 Sesquiterpene gasSOA species notation in the URMELL gas-phase mechanism and SOA module, the molecular weight (MW), reference saturation vapour pressure (p_i^{*R}) and parameter *a* and *b* for calculating the temperature-dependent enthalpy of vaporisation

URMELL species	SOA notation	MW (g mol^{-1})	p_i^{*R} (Pa)	*a* (kJ mol^{-1} K^{-1})	*b* (kJ mol^{-1})	Method
BCNO3	CPBCNO3	283.41	1.24×10^{-3}	−47.511	108 322	i
BCOOH	CPBCOOH	254.41	6.95×10^{-7}	−47.511	132 199	i
P1NO3	CPP1NO3	315.41	6.10×10^{-6}	−54.085	130 188	i
P2NO3	CPP2NO3	331.41	1.0×10^{-10}	−55.181	150 587	i
PSQTOOH	CPPSQTOOH	204.18	1.0×10^{-10}	−55.181	159 458	i
PROD1	CPPROD1	236.39	4.04×10^{-3}	−52.442	107 230	i
PROD2	CPPROD2	252.39	5.00×10^{-6}	−52.442	129 708	i
PROD3	CPPROD3	238.36	5.50×10^{-4}	−52.442	113 735	i
PROD4	CPPROD4	254.36	5.85×10^{-7}	−52.442	136 373	i

daytime component contains a nitro, hydroperoxy and three hydroxyl groups and the night-time component contains a nitro, nitrate, hydroperoxy and two hydroxyl groups. A brief description and schematics of aromatic gasSOA formation for benzene, toluene and xylene are provided in the ESI (Fig. S1-2–S1-4).†

2.2. Explicit gasSOA through phase partitioning of isoprene oxidation products

For isoprene, three gasSOA systems pending on the initial oxidation step emerge: OH, NO_3 and O_3. While OH and NO_3 radical-related oxidation lead to complex systems with a multitude of gasSOA precursor substances (see Fig. S1-5 and S1-6†), O_3 oxidation is implemented to result in only two branches: MVK and MACR (Fig. S1-7†) leading to the gasSOA precursor substances LHMVKABOOH, MACROOH and MACR2NOOH. Note that MVK, MACR and their subsequent reaction products are also part of the OH and NO_3 radical related isoprene gasSOA oxidation schemes. In total, 20 isoprene gasSOA species are included in URMELL and listed in Table 2. Compared to the other gasSOA precursor substances, MVK and MACR reaction products have rather high saturation vapour pressure values which restricts their contribution to the particle-phase. Compounds with multiple hydroperoxy and/or nitrate groups tend to lower saturation vapour pressure values and thus have higher gas-to-particle conversion ratios.

2.3. Explicit gasSOA through phase partitioning of sesquiterpenes oxidation products

The oxidation scheme implemented in URMELL follows Khan *et al.*[99] and includes eight sesquiterpenes SOA species: PROD2, BCNO3, BCOOH, P1NO3, P1OOH, PROD4, P2NO3 and P2OOH. More details about the sesquiterpene scheme including a schematic can be found in Khan *et al.*[99] However, all necessary p_i^{*R} values of sesquiterpene products were re-examined. Instead of the Nannoolal method[95–97] as in Khan *et al.*,[99] here the Myrdal

and Yalkowsky method[92–94] is used, as it provides lower values. As a result, PROD1 and PROD3 are added to the SOA species list and P1OOH turns into a non-volatile compound similar to P2NO3 and P2OOH. Therefore, no chemical reactions are included for P1OOH in URMELL and P1OOH and P2OOH are lumped together into PSQTOOH. Table 3 summarises the sesquiterpene gasSOA species and their corresponding values for molecular weight (MW), the reference vapour pressure p_i^{*R} and the parameters a and b for the $\Delta H_{vap}(T)$ function as implemented in URMELL.

2.4. 2p approach implementation for monoterpenes, alkanes and other alkenes

For monoterpenes, higher alkanes and alkenes (excluding isoprene), a 2p approach is implemented, because of still lacking knowledge and the necessity for further mechanism development. The 2p approach applied is based on SORGAM[68] but was recently extended and considers more SOA pathways for monoterpenes (for more detail see Luttkus *et al.*[28]). Importantly, the 2p approach was designed to be used in conjunction with the gas-phase mechanism RACM[55] and therefore URMELL species have to be transferred to RACM[55] species accordingly (see Table 4).

The lumped URMELL species BIGALK and BIGENE comprise a multitude of various species with varying SOA forming potentials which makes the implementation of the 2p approach designed for the RACM species HC8, OLT and OLI even more challenging. This is especially true for BIGALK which comprises the RACM[55] species HC3, HC5 and HC8, of which only HC8 is considered a SOA precursor. Based on the emission ratios provided by Middleton *et al.*,[100] HC8 contributes about 20% to BIGALK emissions. Therefore, the stoichiometric coefficient for SORGAM[68] was multiplied by 0.2 to only account for the HC8 fraction. Due to the faster OH reaction rate constant of HC8 compared to BIGALK, this value should be seen as a minimum contribution.

3. Model setup

To evaluate the developed semi-explicit SOA module, simulations with the CTM COSMO-MUSCAT[101,102] are performed. To test the semi-explicit SOA formation capacity in comparison to the 2p approach, simulations using the default COSMO-MUSCAT setup (chemical mechanism: extended RACM version[28,55,103] with the pure 2p-SOA approach[28,55]) and the new chemical mechanism URMELL[19] in combination with the presented semi-explicit gas-SOA approach are performed and analysed. Note, that the current set up calculates total SOA mass concentrations and no particle size distribution. Further, there is no separate aqSOA module available for COSMO-MUSCAT yet, therefore only gasSOA can be considered for the explicit SOA estimation neglecting possible aqSOA contributions. The 2p approach of the standard set up includes SOA products from lumped aromatics (xylene, toluene and cresol), higher alkane and alkene, as well as for the reaction of monoterpenes, isoprene and sesquiterpenes.[28] The current simulations build upon the recently performed URMELL gas-phase analysis, therefore, the same setup as for the previous study is used (for more detail on emissions, deposition, spin-up and time period the reader is referred to Luttkus *et al.*[19] and additionally to Luttkus *et al.*[28]). The simulations are carried out for Germany May 2014 to allow for comparison to prior results.[19,28] The model comparison focuses on the 20th of May 2014, because of warm temperatures, high solar radiation and calm winds that favour local SOA formation processes, after a frontal system accompanied with rain passed the model domain on the 19th of May 2014.

Table 4 Corresponding URMELL and RACM species

Parent NMVOC	URMELL species	RACM species
Monoterpenes	APIN, BPIN, LIMONENE, MYRC	API, LIM
Alkanes	BIGALK	HC8
Alkenes	BIGENE	OLT, OLI

4. COSMO-MUSCAT model results

Based upon the extended isoprene and aromatics mechanism development of URMELL,[19] the analysis focuses on the resulting explicit gasSOA scheme for aromatics and isoprene. Map plots of various SOA compounds for 3 UTC, 13 UTC, 19 UTC and 23 UTC of the 20th of May 2014 are shown in S2 and S3.† The analysis of O_3 and OH radical concentrations, the dominant oxidants, has already been presented in Luttkus *et al.*[19] and will not be assessed here again. During the 18th and 19th of May intensive rain events in the east and north of the model domain (Fig. S1-8†) cause stronger trace gas deposition due to subsequent reaction chains and corresponding multiple deposition processes for URMELL compared to the single oxidation step of the 2p approach. Therefore, all URMELL SOA precursor concentrations decline especially in the northeast (Fig. S2-1, S2-2, S3-1 and S3-2†) at 3 UTC. As described in Section 2, the total available organic mass also plays an important role in modulating the gas-to-particle conversion ratio of the SOA precursors and due to the reduction of SOA precursor substances in the north, the total organic absorbing matter is reduced.

4.1. Simulated explicit aromatic gasSOA

For aromatic compounds, different concentration patterns emerge between the 2p and the semi-explicit approach (Fig. 1). The simulation using the 2p approach shows highest aromatic SOA concentrations (CPARO) closer to the emission sources. In the simulation with URMELL, the first oxidation products are transported further away from the sources, whereby oxidative condition changes result into diverse reaction pathways influencing the yield of the SOA precursors.

Interestingly, for the simulations with URMELL, high particle-phase concentration of aromatic SOA is modelled in remote spruce forest areas, *e.g.*, the Harz and Thuringian Forest (Fig. 1a–c) at 3 UTC. Analyses of the formation pathways reveal that NAROMOLOOH is the main contributor to total aromatic SOA (Fig. 2 and S2-6–S2-8†). NAROMOLOOH is a non-volatile end product formed after at least five to six PHENOL

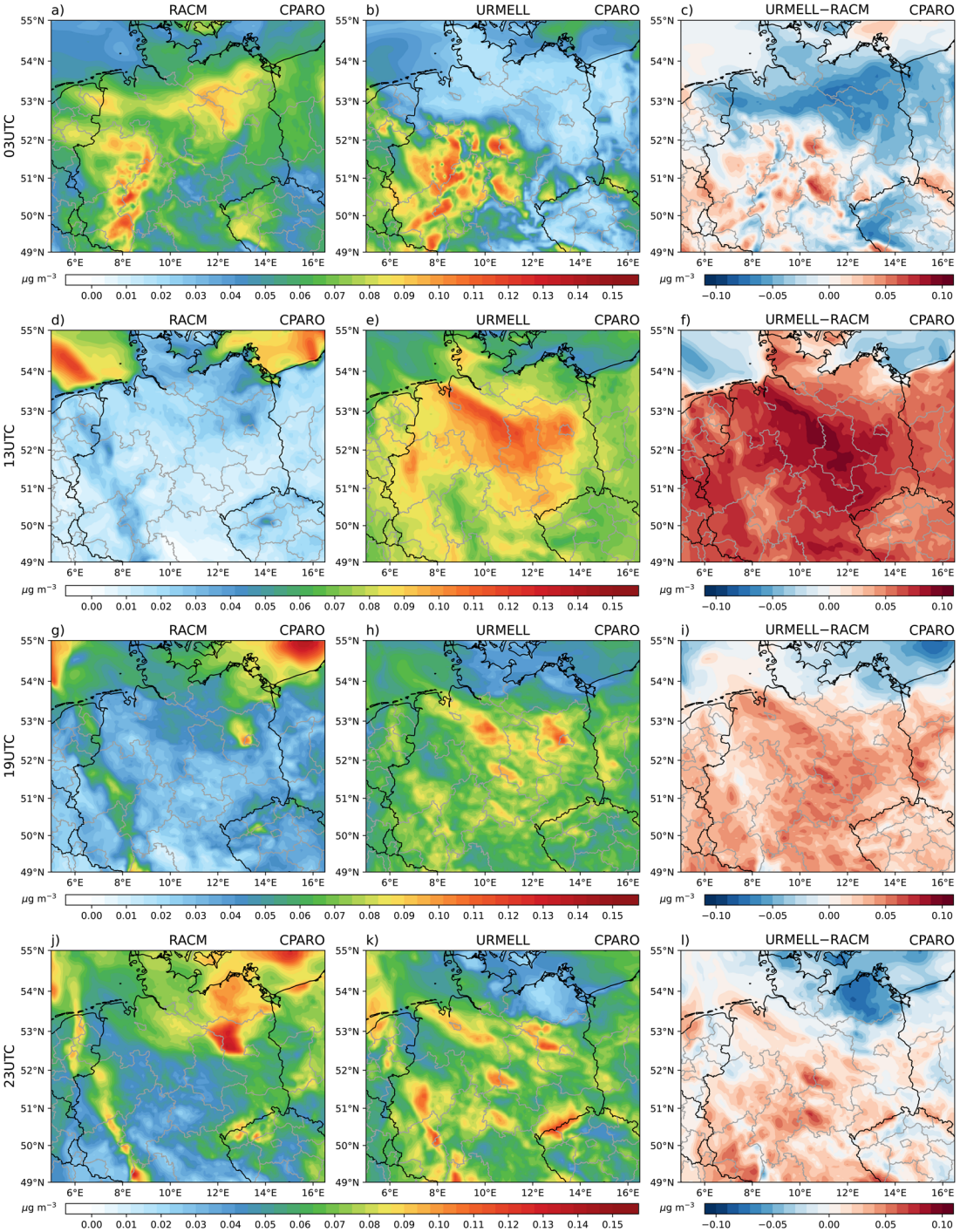

Fig. 1 Total aromatic particle-phase concentration on the 20th of May 2014 for RACM (a, d, g and j); URMELL (b, e, h and k); difference between URMELL and RACM (c, f, i and l) for 3 UTC, 13 UTC, 19 UTC and 23 UTC respectively.

oxidation steps (Fig. S1-2†). The dominant path to form NAROMOLOOH is from oxidation of phenol to NPHEN and later NPHEN oxidation to N2PHEN (Fig. S1-2†). NPHEN occurrence is closely linked to phenol and NO_2 emission sources with only minor contributions in remote areas. The further oxidation of NPHEN and subsequent reaction with NO_2 results into N2PHEN. It is important to note that NPHEN and N2PHEN react very rapidly with the NO_3 radical that is the dominant radical during night. The distribution of N2PHEN starts to switch towards spruce forests, where due to low night-time monoterpene emissions high NO_3 concentrations are reached.[28] As a consequence, rapid N2PHEN oxidation occurs at 3, 19 and 23 UTC which is a NAROMOLOOH precursor. Even though HO_2 is low in concentration during night, the spruce forest oxidising conditions in the Harz and Thuringia Forest still lead to NAROMOLOOH formation (Fig. 2 and S2-6–S2-8†).

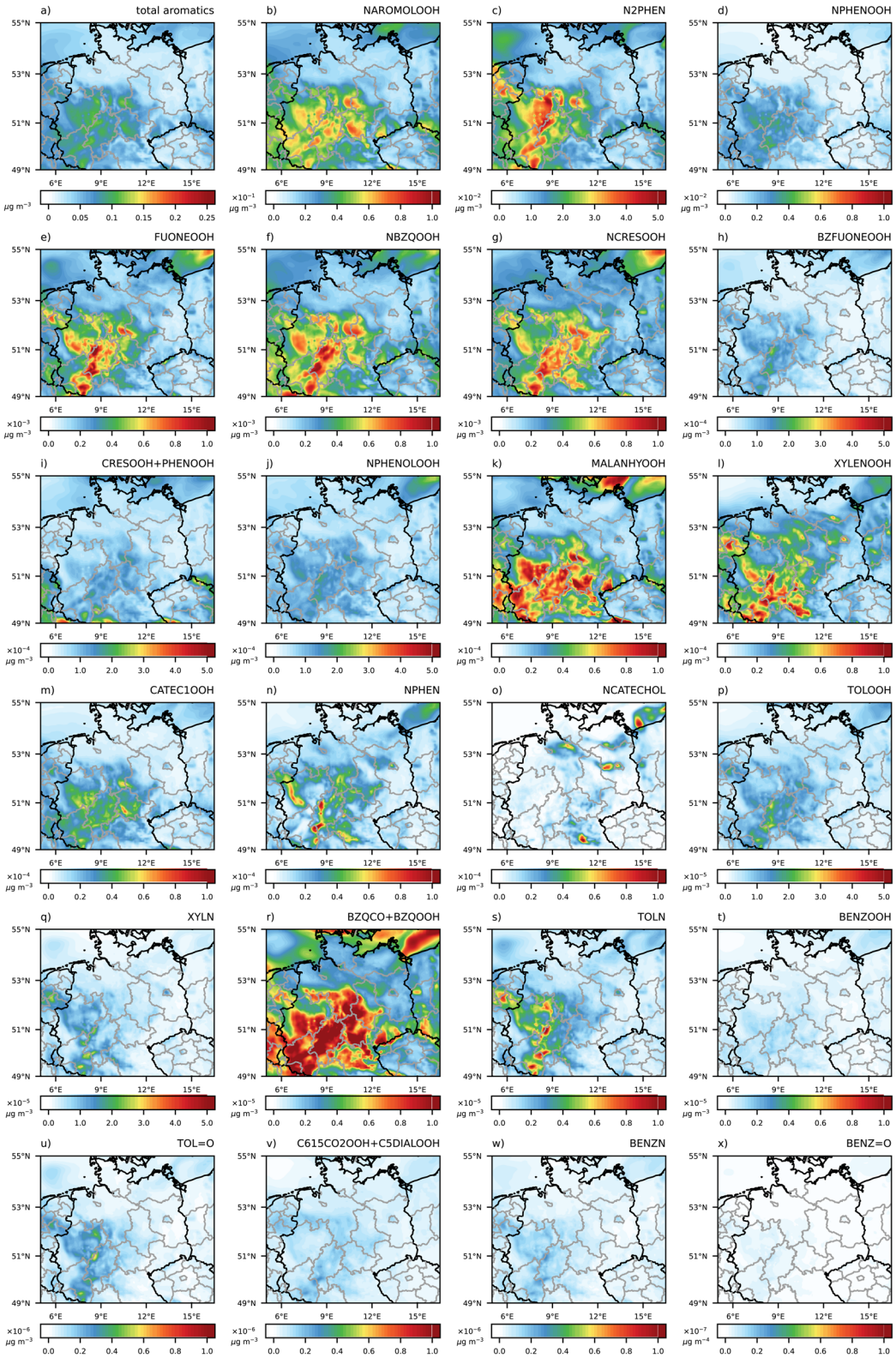

Fig. 2 Contribution of the individual aromatic gasSOA precursor substances to the particle phase at 3 UTC. Note, the changing magnitude of the individual figures starting with the highest concentrations.

During the day, URMELL outcompetes the aromatic particle concentration simulated with the 2p approach, except for the Northern and Baltic Sea (Fig. 1). The total concentration of aromatic SOA precursor concentration (Fig. S2-1†) is higher in the simulation with URMELL for most parts of the model domain except the area impacted by heavy rain in the north east

at 3 UTC, the maritime areas for all time steps and an area along the river Rhine. These differences are caused by multiple factors: (i) advection processes, (ii) shift of SOA production from first oxidation to subsequent reaction steps, (iii) change in saturation vapour pressure values and (iv) missing SOA sources which will be addressed hereafter. Due to advection, the higher SOA concentrations for the simulation using the 2p approach in the north of the domain are transported northward towards the North and Baltic Sea, serving as additional sources which are missing for URMELL due to the very low simulated concentrations in this rain affected areas. The immediate SOA production of the 2p approach is likely the cause for the higher aromatic SOA and precursor concentration along the river Rhine for the simulation using the 2p approaches. This area is dominated by anthropogenic emissions originating from ships and the high density of industrial and urban areas.

Different to these model findings, the high night-time occurrence of NAROMOLOOH in spruce forest regions illustrates the necessity to consider entire degradation sequences under varying oxidant conditions throughout the transport process. This finding is reinforced by box model results from an urban outflow plume, which support a high NAROMOLOOH night-time production.[104] An immediate approximation at the first oxidation step does neither cover the contribution nor the distribution as simulated with the explicit approach well. Due to longer atmospheric lifetimes of aromatic compounds compared to BVOCs using the reaction rate constants provide in URMELL[19] and the $OH/NO_3/O_3$ concentrations provided by Atkinson & Arey,[26] transport processes are of high importance. Furthermore, the implementation of the non-volatile product NAROMOLOOH makes aromatic SOA approximation with URMELL more efficient, as this allows for continuous SOA production, independent of the total absorbing organic matter, which is crucial for the 2p approach. So far, the simulation using URMELL is only capable of gasSOA modelling, which neglects several aqSOA contributions. However, possible aqSOA precursor substances such as maleic anhydride (MALANHY) which hydrolyse in aqueous solutions yielding maleic acid[85,105–107] are already included in the URMELL chemical mechanism. Adding MALANHY to the SOA precursor concentration further enhances the URMELL precursor concentration (Fig. S2-1†). The concentration pattern of MALANHY (Fig. 3) is in very good agreement with the 13, 19 and 23 UTC RACM ARO prediction (Fig. S2-1†).

The contribution of the individual aromatic precursor substances changes over the course of the day (Fig. S2-2–S2-5†) but NAROMOLOOH and N2PHEN appear most frequently and with highest concentrations. The formation of gasSOA precursor products with a remaining aromatic ring structure NPHENOOH and CATEC1OOH (Fig. S1-2†) are linked to ozone oxidation and present throughout the day. A clear daytime component (high for 13 UTC, lower for 19, 23 and 3 UTC) show products such as NCATECHOL which require OH oxidation steps, while products solely generated *via* NO_3 pathways (NCRESOOH, NPHENOLOOH) have a strong night-time component. For intermediate products (*e.g.* furanones and quinones) with unequal OH and NO_3 lifetimes ($k_{NO_3} > k_{OH}$) the reaction products accumulate during the day due to inefficient OH oxidation shifting further degradation processes into the night, when sufficient concentration levels of NO_3 build up. Therefore, the SOA contribution of *e.g.* FUONEOOH, NBZQOOH, BZFUONEOOH is highest at 3 UTC (Fig. 2).

4.2. Simulated explicit isoprene gasSOA

Different to aromatics, similar patterns between the 2p and the semi-explicit approach are simulated for isoprene at all time steps considered (Fig. 4). Both simulations show highest isoprene gasSOA concentrations (CPISO) in the west of the domain and north of Berlin where high portions of oaks emit huge quantities of isoprene.

The four most abundant isoprene-related SOA precursor substances modelled are NISOPOOHOH=O, LISOPNO3NO3, LISOPNO3OOH and IHNEOOH (Fig. S3-2–S3-5†). Except for IHNEOOH, which originates from initial isoprene NO_3 oxidation favoured during night, all have OH and NO_3 oxidation related formation pathways and are therefore present throughout the entire modelled day (see Fig. S1-5–S1-7†). However, based on the products formed, specific conclusions on the oxidative state of the troposphere can be drawn:

- NISOPNOOH, MACRNOOH and IHNEOOH generally originate from initial NO_3 radical-related oxidation of isoprene.
- LISOPNO3NO3 only forms under very high NO concentrations.
- DHPMEK, DHPMPAL and DHHPEPOX are produced under high HO_x and low NO_x conditions.
- LISOPOOHOOH requires two HO_2 oxidation steps also dementing high HO_x concentrations.

At the moment, no conclusion on O_3 oxidation processes are possible, as both primary products formed (MVK, MACR) together with their subsequent reaction products have also additional OH and NO_3 radical related isoprene oxidation pathways. In the following, detailed analyses of the modelled

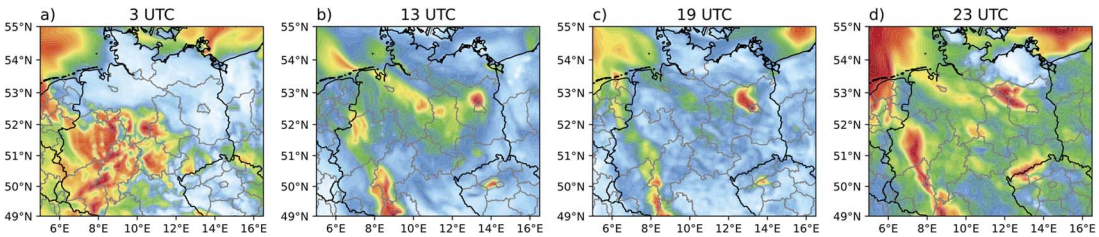

Fig. 3 MALANHY gas-phase concentration pattern for (a) 3 UTC, (b) 13 UTC, (c) 19 UTC and (d) 23 UTC.

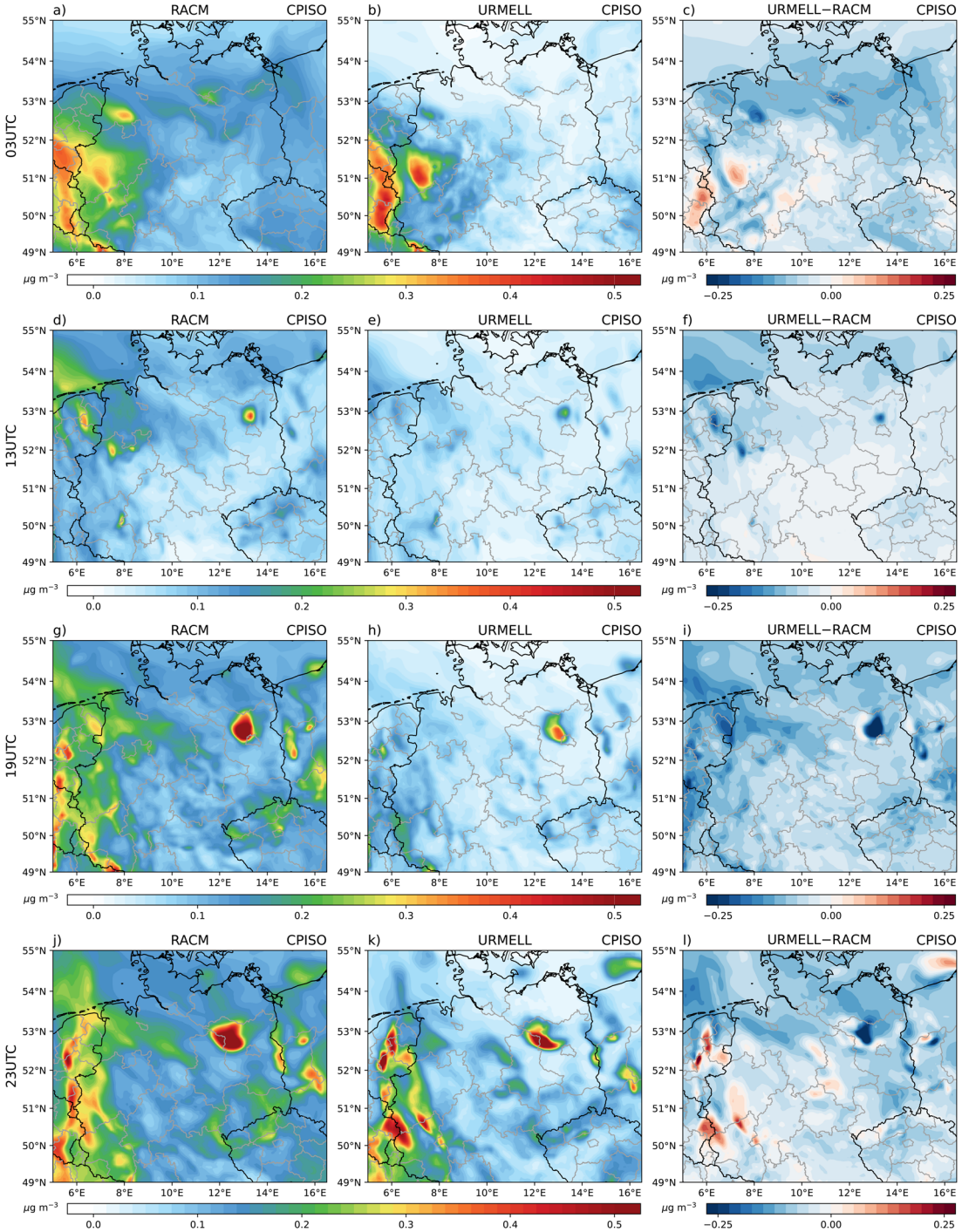

Fig. 4 Total isoprene particle-phase concentration (CPISO) on the 20th of May 2014 for RACM (a, d, g and j); URMELL (b, e, h and k); difference between URMELL and RACM (c, f, i and l) for 3 UTC, 13 UTC, 19 UTC and 23 UTC respectively.

concentrations are provided. In general, the same factors as stated in Section 4.1 apply (advection, subsequent reaction chains, change in saturation vapour pressure values, missing SOA).

Again, due to southerly winds with an easterly component in the north of the domain, higher 2p concentrations are advected north-west bound. More frequent isoprene emission sources[28] in the west of the domain enhances the advection effect over the North Sea for all time steps (Fig. 4). In the east, an isolated spot north of Berlin is present. At 13 UTC, the 2p approach produces higher SOA precursor concentrations closer to Berlin in close approximation to the isoprene emission source of an oak forest due to the immediate SOA formation while URMELL produces higher concentrations further along the trajectory north of the forest. A slight increase in wind velocity and change in direction cause a stronger deviation for 19 UTC with again higher 2p concentrations north of Berlin but higher URMELL concentrations to the west. The lack of night-time isoprene emissions

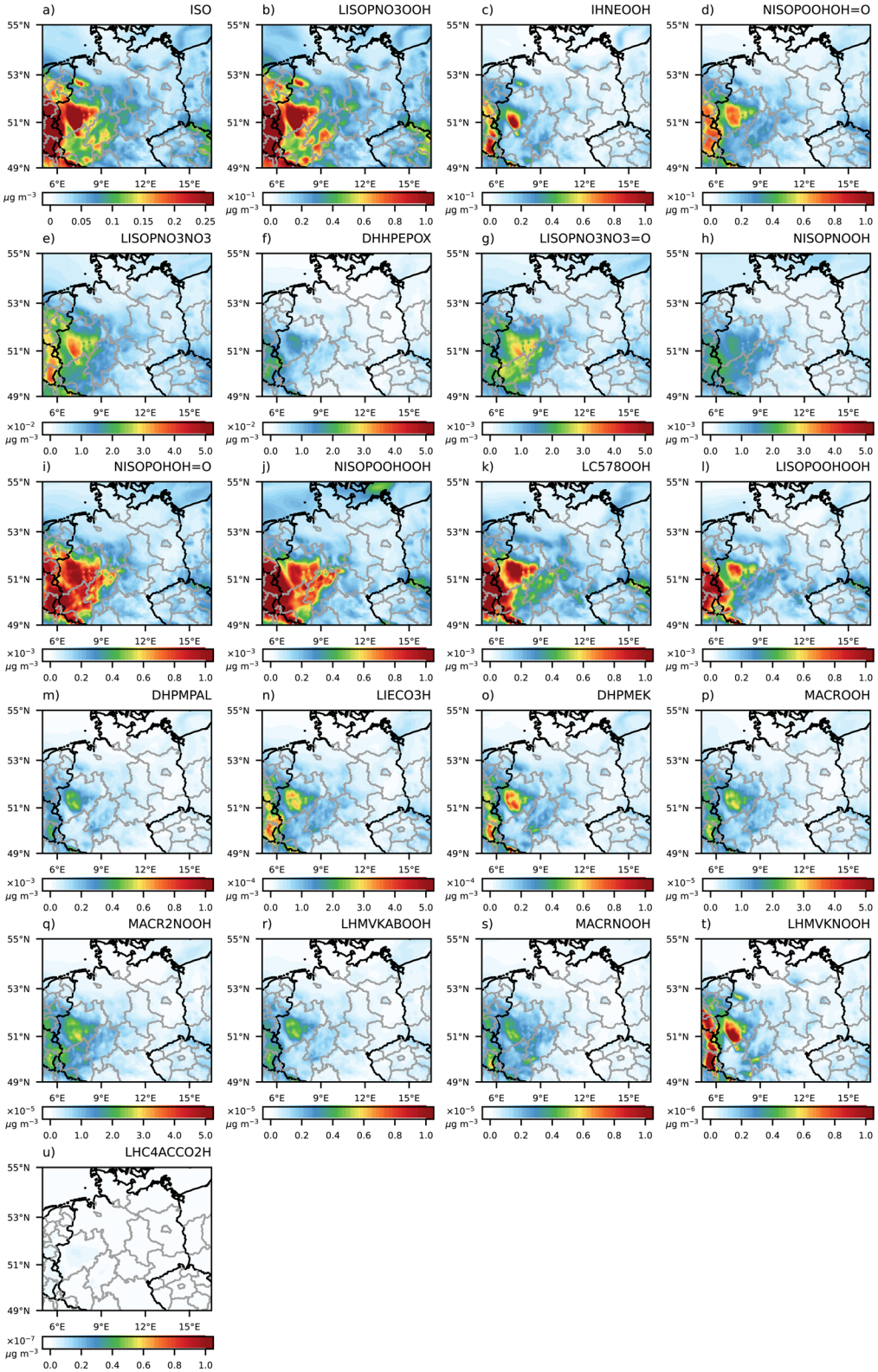

Fig. 5 Contribution of the individual isoprene SOA precursor substances to the particle-phase at 3 UTC. Note the changing magnitude of the individual figures starting with the highest concentrations.

reduces these deviations at 23 UTC. Note that due to the southerly winds, this area is also influenced by NO_x outflow from Berlin.

For isoprene, possible important aqSOA formation processes by isoprene-related epoxides[62] lumped into LIEPOX in URMELL and HMML[108,109] are not included in MUSCAT, yet. Adding

LIEPOX and HMML enhances the isoprene SOA precursor concentration, but in the case of the two spots with lower difference values at 3 UTC only a marginal increase can be observed (Fig. S3-1d and S3-2†). For 13 and 19 UTC LIEPOX (Fig. S3-3v and S3-4v†) and HMML (Fig. S3-3w and S3-4w†) show individual contributions similar or even higher than the most abundant gasSOA precursor NISOPOOHOH=O (Fig. S3-3d and S3-4d†). As a result, a significant increase in total URMELL SOA precursor concentration would be reached for nearly the entire model domain (Fig. S3-1†). At 13, 19 and 23 UTC, highest deviations between URMELL and the 2p approach simulated isoprene particle (Fig. 4) and total SOA precursor concentrations (Fig. S3-1†) appear in the north of the domain especially the North Sea and north of Berlin. Mainly driven by the already discussed transport-related effects and the NO_x dependency of the SOA yield, here, including LIEPOX (Fig. S3-3v and S3-4v†) and HMML (Fig. S3-3w and S3-4w†) enhances the isoprene SOA precursor concentration. While LIEPOX is linked to high HO_x and NO, HMML is linked to HO_x and NO_2 concentrations, whereby indicating areas of possible NO_x dependent over and under predicted 2p SOA estimations. Especially for Berlin, the southerly and south-easterly winds transport high urban NO_x concentration from Berlin northward towards the high isoprene emitting oak forest promoting LIEPOX and HMML in close approximation.

Overall, an increase in URMELL CPISO concentration is only reached at 3 and 23 UTC (Fig. 4) in areas where higher isoprene precursor (Fig. S3-1†) and similar or higher CPARO values (Fig. 1) are reached. IHNEOOH shows high quantities at both time steps and its concentration pattern (Fig. 5 and S3-8†) shows similarities to areas with higher simulated URMELL CPISO values (Fig. 4c and l). Otherwise URMELL simulates lower CPISO concentrations than the 2p approach. Especially in the north, lower CPISO values are reached, where washout processes reduce the total amount of OM. As isoprene is only emitted during the day, night-time SOA and SOA precursor

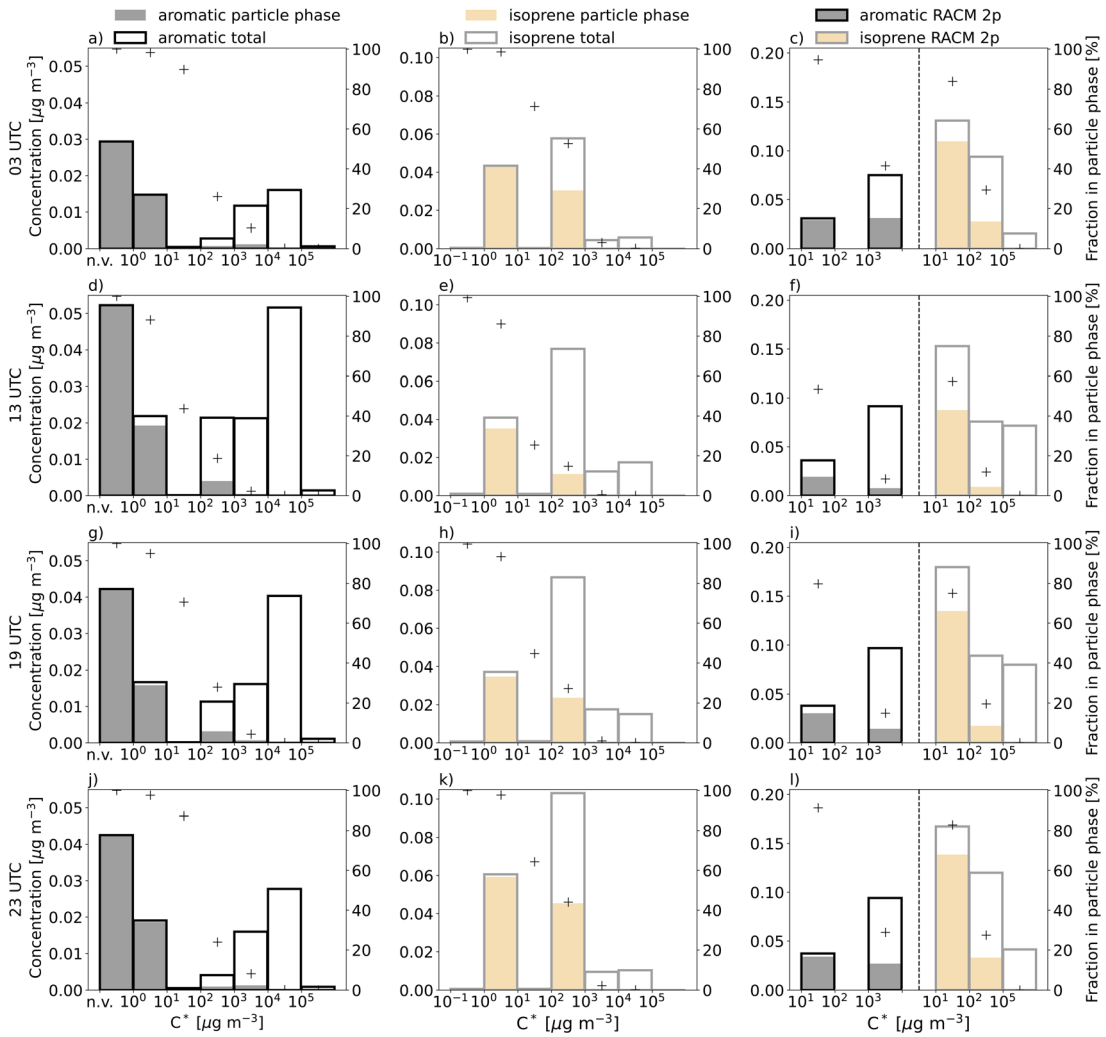

Fig. 6 Spatial mean total gasSOA precursor and particle-phase concentration of URMELL aromatic (a, d, g and j), URMELL isoprene (b, e, h and k) as well as RACM 2p aromatic and isoprene (c, f, i and l) related organic mass concentration transferred to individual volatility bins C^* as used for the VBS approach (bins sum up all products between the previous value and the current volatility bin value, n.v. stands for non-volatile) on the 20th of May 2014 at 3, 13, 19 and 23 UTC, respectively. Additionally, shown is the fraction in the particle phase by black crosses.

patterns are influenced by advection processes rather than direct emissions. Even though, the oxidation of isoprene is rather fast during the day a shift along transport trajectories combining the impact of stepwise oxidation steps for varying environmental conditions and the production of individual products formed with transport related processes are evident especially at 23 UTC (Fig. 4).

4.3. Advances of an explicit gasSOA approach

The above performed comparisons between a standard 2p and the new explicit approach for simulated SOA from oxidation of aromatic compounds and isoprene revealed that simulations using URMELL result into an increase of modelled CPARO, but lower modelled CPISO gasSOA concentration. However, the CPISO concentration might be equally if aqSOA formation from

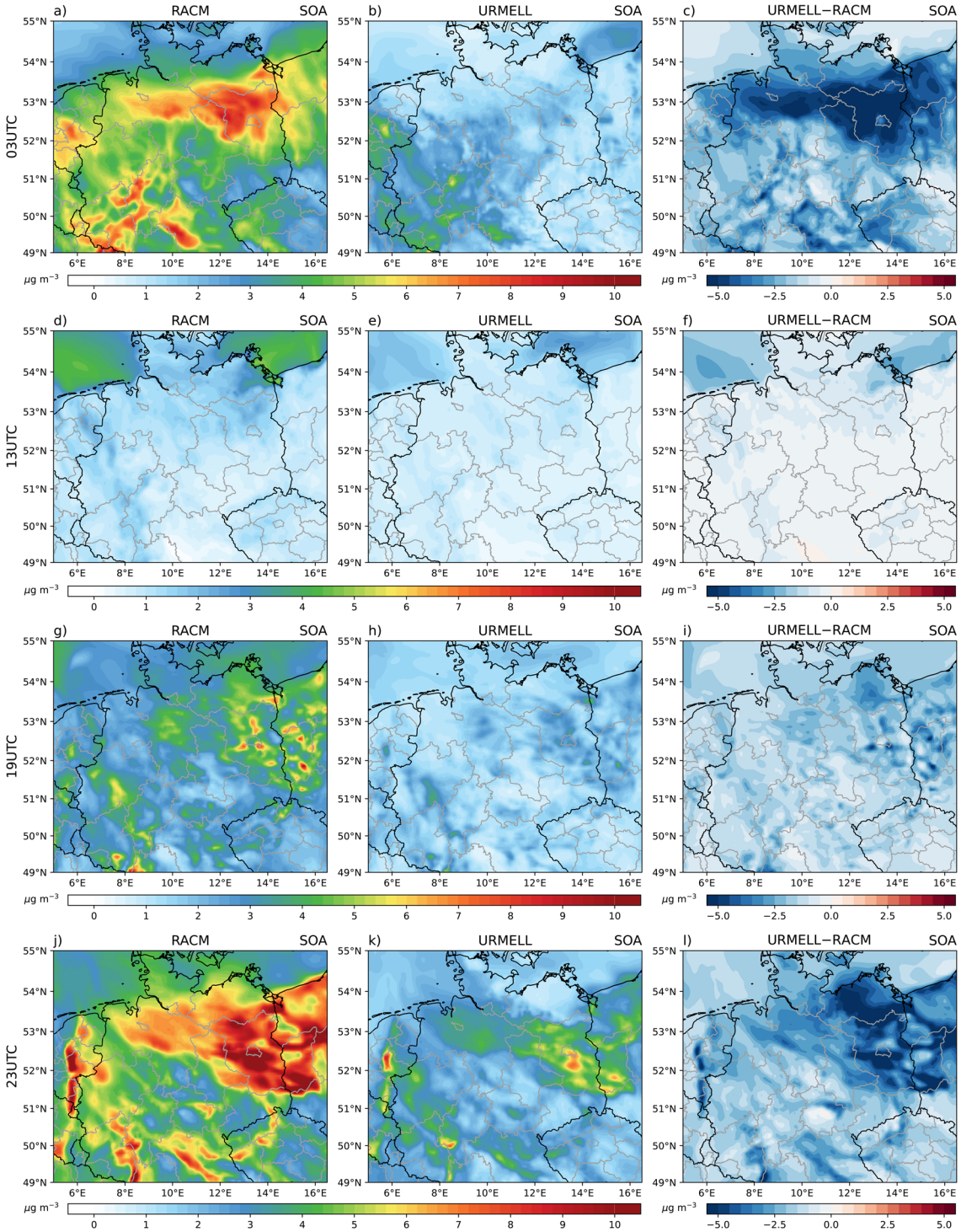

Fig. 7 Total particle-phase concentration (SOA) on the 20th of May 2014 for RACM (a, d, g and j); URMELL (b, e, h and k); difference between URMELL and RACM (c, f, i and l) for 3 UTC, 13 UTC, 19 UTC and 23 UTC respectively.

LIEPOX and HMML would be considered by the model. The model approach of aqSOA formation is only valid for URMELL as for a 2p approach, no differentiation between gasSOA and aqSOA is possible, but may be part of the parameterisation. The creation of a detailed yet compact aqSOA description in MUSCAT is beyond the scope of the present study, but is part of future model developments.

Still, specific advancements of the new scheme where detected that are further outlined in this section. The explicit aromatics and isoprene SOA modelling scheme using URMELL delays the actual formation of SOA from the first initial oxidation step as applied for 2p/VBS approaches towards subsequent oxidation steps whereby considering multi-generation products for varying environmental conditions. This shifts SOA formation processes along transport trajectories. For aromatics, the longer lifetime of the reaction products results often into the uncoupling of areas with high CPARO from the emission sources. This is especially modelled through the integration of NO_3 pathways resulting in high night-time concentrations in spruce and beech forest areas (Fig. 1 and S2-1†). For isoprene, SOA formation processes also shift along the trajectories, resulting in areas of negative and positive difference values (Fig. 4 and S3-1†) in close proximity (*e.g.* north of Berlin).

Besides these advection/transport related effects, the contribution of a diversity of explicit SOA precursors and the knowledge about their individual properties (vapour pressure, molecular weight, *etc.*) and functional group composition can provide more insights into their impacts on cloud and precipitation formation processes. These processes are governed by the physico-chemical properties of aerosol particles that include hygroscopicity (related to the chemical composition) and the size- and number distribution. In the simulations, the overall contribution of aromatics to total organic mass is smaller than for isoprene, but oxidation of aromatics leads to a higher portion of very low and non-volatile compounds which can participate in new particle formation while isoprene leads to higher quantities of more volatile products facilitating particle growth (Fig. 6).

4.4. Total gasSOA concentration

Even though, the development of URMELL was focussed on establishing an explicit aromatic and isoprene scheme, sesquiterpene, monoterpene, alkane and alkene SOA production are considered, too and were presented in Sections 2.3 and 2.4. These are necessary to create organic mas for gas-/particle partitioning. Here, the 2p approach is mainly used and the results are briefly presented in the ESI S1.2 and map plots are provided in S4.†

For both simulations, the oxidation of monoterpenes represents the major SOA source. Sesquiterpenes, isoprene, aromatics and alkanes have comparable modelled effects on SOA concentration levels, while alkenes show the lowest contribution. Therefore, especially the reduction in monoterpene SOA concentration within the URMELL simulation impacts the total available absorbing organic mass. This results into significantly lower partitioning from the gas- into the particle-phase for all SOA precursor substances and reduces the total SOA concentration simulated with URMELL (Fig. 7). Overall, the reduction of monoterpenes, sesquiterpenes, alkanes and alkenes SOA contribution results in halved averaged total SOA concentration with URMELL (1.49 μg m^{-3} compared to 3.03 μg m^{-3} with RACM 2p) for the 20th of May 2014. Thereof, CPARO (0.06/0.046 μg m^{-3}) and CPISO (0.066/0.16 μg m^{-3}) contribute 4%/1.5% and 4.4%/5.3% respectively. Sesquiterpenes (0.06/0.17 μg m^{-3}), monoterpenes (1.29/2.45 μg m^{-3}), alkanes (0.006/0.21 μg m^{-3}) and alkenes (0.002/0.01 μg m^{-3}) contribute 4%/5.6%, 86.6%/81%, 0.4%/7%, 0.1%/0.3%, respectively.

5. Conclusion

Within the present study, two explicit gasSOA modelling schemes one for aromatics and one for isoprene have been developed and presented together for use with the chemical mechanism URMELL.[19] The parameterisations are designed as such that they can be implemented into other detailed chemical mechanisms. The switch from the first oxidation step SOA approximation to subsequent oxidation steps allows the consideration of a multitude of low to non-volatile reaction products whereby considering changing environmental conditions such as the NO_x regime along transport trajectories. With such an approach, SOA formation far away from the emission source can be detected and put into different, possibly more realistic, context. For example, the inclusion of NO_3 pathways into aromatics oxidation scheme revealed a link between anthropogenic emissions, transport processes and taxonomic biodiversity driven impacts through high night-time aromatic SOA concentrations in beech and spruce forests. Similar to Lee-Taylor *et al.*,[104] MALANHYOOH and NAROMOLOOH were identified as multi-generation reaction products with significant ASOA contributions.

This study, acknowledges the findings from Lee-Taylor *et al.*[104] for urban and forest outflow box model simulations and raises the knowledge to a regional scale confirming a potentially larger spatial impact of ASOA than previously thought. Further, there is evidence from measurements, that even in remote areas a considerable amount of SOA is formed *via* anthropogenic precursors or NO_x-dependent BSOA pathways.[45,46,110,111]

The analysis of the simulated gasSOA composition reveals different SOA pathways and consequently varying products for HO_x and NO_x dominated regimes with individual characteristics (*e.g.* chemical composition, hygroscopicity, volatility). In comparison to simulations with the 2p approach, the higher amount of non-volatile aromatic reaction products increases the aromatic SOA concentration despite the lower overall SOA concentration. This highlights the importance of an adequate volatility representation for SOA modelling as the choice of the volatility class determines its gas-to-particle partitioning dependency on the total absorbing organic matter.

Besides the obvious impact on particle mass the simulation results can be used for other important features such as particle composition, number and size distribution. With this, cloud and precipitation formation processes could be further quantified. A recent study emphasises the importance of treating biogenic SOA in ESM to be essential for estimating the forest

aerosol–cloud–climate feedbacks.[35] In conjunction with the knowledge gained in this analysis it is shown that quantification of adequate volatility classes and identification of important SOA products and pathways can help to overcome current model uncertainties and constrains. The advances of an explicit gasSOA approach has been displayed here for aromatics and isoprene reaction products, but to further elaborate and evaluate the findings, detailed knowledge about the individual SOA components of measured aerosol concentrations are required, which are difficult to identify. Further, the current model restriction to gasSOA neglects possible aqSOA contributions (*e.g.* MALANHY, IEPOX, HMML) reducing the total SOA formation potential of URMELL in comparison to solely using the 2p approach. Possible aqSOA contributions to the SOA precursor concentration were discussed revealing high IEPOX and HMML in the urban outflow plume of Berlin and high MALANHY contributions closer to the emission sources comparable with the 2p pattern.

Here, we demonstrate that it is possible to simulate a detailed SOA parameterisation in CTMs using the model framework COSMO-MUSCAT with URMELL. Compared to the RACM-2p simulation the number of species, chemical reactions and SOA products increased significantly and as a consequence the computation time increased (roughly doubles). Further, SOA formation is no longer decoupled from chemical processes but rather a direct result from the underlying chemical mechanism URMELL enabling direct oxidant feedback. Therefore, such detailed CTM simulation analysis may help to define the degree of sophistication needed to adequately describe SOA formation processes for a variety of precursors also for use in ESMs to improve simulated aerosol–cloud–climate feedbacks, which still show significant model uncertainties.[35]

The results presented confirm the feasibility of and lay the foundation for an explicit SOA modelling approach. Extending the explicit SOA scheme to monoterpenes, alkane and alkene, as well as the aqueous-phase requires further chemical mechanism as well as SOA scheme development and will be addressed in the near future. Also, the formation of stable accretion products (ROOR and dimers) from the reaction of two peroxy radicals have been identified to yield ultralow volatile compounds[41,75–81] and will be included over the course of future model development steps.

All in all, the current advancements highlight the urgent need to further improve our understanding of anthropogenic and biogenic interactions which is essential for robust air quality and climate mitigation strategy predictions and to quantify man-made air quality and climate impacts.

Data availability

Model simulation data of the 2p- and semi-explicit URMELL gasSOA approach for the 20th of May 2014 are available at Zenodo at **https://doi.org/10.5281/zenodo.11444412**.

Author contributions

Conceptualization: MLL, RW, AT, EHH. Data curation: MLL. Formal analysis: MLL. Funding acquisition: MLL. Investigation: MLL. Methodology: MLL, RW, AT, EHH. Project administration: MLL, RW. Software: MLL, RW. Supervision: MLL, RW. Validation: MLL. Visualization: MLL, JW. Writing – original draft: MLL. Writing – review & editing: MLL, JW, EHH, AT, RW, HH, IT.

Conflicts of interest

There are no conflicts to declare.

Acknowledgements

This work was funded by the PhD scholarship of the German Federal Environmental Foundation (Deutsche Bundesstiftung Umwelt, DBU) granted to MLL (AZ 20016/452).

References

1 K.-H. Kim, E. Kabir and S. Kabir, A review on the human health impact of airborne particulate matter, *Environ. Int.*, 2015, **74**, 136–143.
2 P. Thangavel, D. Park and Y.-C. Lee, Recent Insights into Particulate Matter (PM2.5)-Mediated Toxicity in Humans: An Overview, *Int. J. Environ. Res. Public Health*, 2022, **19**, 7511.
3 E. von Schneidemesser, P. S. Monks, J. D. Allan, L. Bruhwiler, P. Forster, D. Fowler, A. Lauer, W. T. Morgan, P. Paasonen, M. Righi, K. Sindelarova and M. A. Sutton, Chemistry and the Linkages between Air Quality and Climate Change, *Chem. Rev.*, 2015, **115**, 3856–3897.
4 J. R. Odum, T. Hoffmann, F. Bowman, D. Collins, R. C. Flagan and J. H. Seinfeld, Gas/Particle Partitioning and Secondary Organic Aerosol Yields, *Environ. Sci. Technol.*, 1996, **30**, 2580–2585.
5 J. F. Pankow, An absorption model of gas/particle partitioning of organic compounds in the atmosphere, *Atmos. Environ.*, 1994, **28**, 185–188.
6 R. Atkinson, Atmospheric chemistry of VOCs and NOx, *Atmos. Environ.*, 2000, **34**, 2063–2101.
7 A. B. Guenther, X. Jiang, C. L. Heald, T. Sakulyanontvittaya, T. Duhl, L. K. Emmons and X. Wang, The Model of Emissions of Gases and Aerosols from Nature version 2.1 (MEGAN2.1): an extended and updated framework for modeling biogenic emissions, *Geosci. Model Dev.*, 2012, **5**, 1471–1492.
8 T. Jokinen, T. Berndt, R. Makkonen, V.-M. Kerminen, H. Junninen, P. Paasonen, F. Stratmann, H. Herrmann, A. B. Guenther, D. R. Worsnop, M. Kulmala, M. Ehn and M. Sipilä, Production of extremely low volatile organic compounds from biogenic emissions: measured yields and atmospheric implications, *Proc. Natl. Acad. Sci. U. S. A.*, 2015, **112**, 7123–7128.
9 K. Lehtipalo, C. Yan, L. Dada, F. Bianchi, M. Xiao, R. Wagner, D. Stolzenburg, L. R. Ahonen, A. Amorim, A. Baccarini, P. S. Bauer, B. Baumgartner, A. Bergen, A.-K. Bernhammer, M. Breitenlechner, S. Brilke,

A. Buchholz, S. B. Mazon, D. Chen, X. Chen, A. Dias, J. Dommen, D. C. Draper, J. Duplissy, M. Ehn, H. Finkenzeller, L. Fischer, C. Frege, C. Fuchs, O. Garmash, H. Gordon, J. Hakala, X. He, L. Heikkinen, M. Heinritzi, J. C. Helm, V. Hofbauer, C. R. Hoyle, T. Jokinen, J. Kangasluoma, V.-M. Kerminen, C. Kim, J. Kirkby, J. Kontkanen, A. Kürten, M. J. Lawler, H. Mai, S. Mathot, R. L. Mauldin, U. Molteni, L. Nichman, W. Nie, T. Nieminen, A. Ojdanic, A. Onnela, M. Passananti, T. Petäjä, F. Piel, V. Pospisilova, L. L. J. Quéléver, M. P. Rissanen, C. Rose, N. Sarnela, S. Schallhart, S. Schuchmann, K. Sengupta, M. Simon, M. Sipilä, C. Tauber, A. Tomé, J. Tröstl, O. Väisänen, A. L. Vogel, R. Volkamer, A. C. Wagner, M. Wang, L. Weitz, D. Wimmer, P. Ye, A. Ylisirniö, Q. Zha, K. S. Carslaw, J. Curtius, N. M. Donahue, R. C. Flagan, A. Hansel, I. Riipinen, A. Virtanen, P. M. Winkler, U. Baltensperger, M. Kulmala and D. R. Worsnop, Multicomponent new particle formation from sulfuric acid, ammonia, and biogenic vapors, *Sci. Adv.*, 2018, **4**, eaau5363.

10 J. Kirkby, J. Duplissy, K. Sengupta, C. Frege, H. Gordon, C. Williamson, M. Heinritzi, M. Simon, C. Yan, J. Almeida, J. Tröstl, T. Nieminen, I. K. Ortega, R. Wagner, A. Adamov, A. Amorim, A.-K. Bernhammer, F. Bianchi, M. Breitenlechner, S. Brilke, X. Chen, J. Craven, A. Dias, S. Ehrhart, R. C. Flagan, A. Franchin, C. Fuchs, R. Guida, J. Hakala, C. R. Hoyle, T. Jokinen, H. Junninen, J. Kangasluoma, J. Kim, M. Krapf, A. Kürten, A. Laaksonen, K. Lehtipalo, V. Makhmutov, S. Mathot, U. Molteni, A. Onnela, O. Peräkylä, F. Piel, T. Petäjä, A. P. Praplan, K. Pringle, A. Rap, N. A. D. Richards, I. Riipinen, M. P. Rissanen, L. Rondo, N. Sarnela, S. Schobesberger, C. E. Scott, J. H. Seinfeld, M. Sipilä, G. Steiner, Y. Stozhkov, F. Stratmann, A. Tomé, A. Virtanen, A. L. Vogel, A. C. Wagner, P. E. Wagner, E. Weingartner, D. Wimmer, P. M. Winkler, P. Ye, X. Zhang, A. Hansel, J. Dommen, N. M. Donahue, D. R. Worsnop, U. Baltensperger, M. Kulmala, K. S. Carslaw and J. Curtius, Ion-induced nucleation of pure biogenic particles, *Nature*, 2016, **533**, 521–526.

11 F. Riccobono, S. Schobesberger, C. Scott, J. Dommen, I. Ortega, L. Rondo, J. Almeida, A. Amorim, F. Bianchi, M. Breitenlechner, A. David, A. Downard, E. Dunne, J. Duplissy, S. Ehrhart, R. Flagan, A. Franchin, A. Hansel, H. Junninen, M. Kajos, H. Keskinen, A. Kupc, A. Kürten, A. Kvashin, A. Laaksonen, K. Lehtipalo, V. Makhmutov, S. Mathot, T. Nieminen, A. Onnela, T. Petäjä, A. Praplan, F. Santos, S. Schallhart, J. Seinfeld, M. Sipilä, D. Spracklen, Y. Stozhkov, F. Stratmann, A. Tomé, G. Tsagkogeorgas, P. Vaattovaara, Y. Viisanen, A. Vrtala, P. Wagner, E. Weingartner, H. Wex, D. Wimmer, K. Carslaw, J. Curtius, N. Donahue, J. Kirkby, M. Kulmala, D. Worsnop and U. Baltensperger, Oxidation products of biogenic emissions contribute to nucleation of atmospheric particles, *Science*, 2014, **344**, 717–721.

12 F. Bianchi, J. Tröstl, H. Junninen, C. Frege, S. Henne, C. R. Hoyle, U. Molteni, E. Herrmann, A. Adamov, N. Bukowiecki, X. Chen, J. Duplissy, M. Gysel, M. Hutterli, J. Kangasluoma, J. Kontkanen, A. Kürten, H. E. Manninen, S. Münch, O. Peräkylä, T. Petäjä, L. Rondo, C. Williamson, E. Weingartner, J. Curtius, D. R. Worsnop, M. Kulmala, J. Dommen and U. Baltensperger, New particle formation in the free troposphere: a question of chemistry and timing, *Science*, 2016, **352**, 1109–1112.

13 J. Tröstl, W. K. Chuang, H. Gordon, M. Heinritzi, C. Yan, U. Molteni, L. Ahlm, C. Frege, F. Bianchi, R. Wagner, M. Simon, K. Lehtipalo, C. Williamson, J. S. Craven, J. Duplissy, A. Adamov, J. Almeida, A.-K. Bernhammer, M. Breitenlechner, S. Brilke, A. Dias, S. Ehrhart, R. C. Flagan, A. Franchin, C. Fuchs, R. Guida, M. Gysel, A. Hansel, C. R. Hoyle, T. Jokinen, H. Junninen, J. Kangasluoma, H. Keskinen, J. Kim, M. Krapf, A. Kürten, A. Laaksonen, M. Lawler, M. Leiminger, S. Mathot, O. Möhler, T. Nieminen, A. Onnela, T. Petäjä, F. M. Piel, P. Miettinen, M. P. Rissanen, L. Rondo, N. Sarnela, S. Schobesberger, K. Sengupta, M. Sipilä, J. N. Smith, G. Steiner, A. Tomè, A. Virtanen, A. C. Wagner, E. Weingartner, D. Wimmer, P. M. Winkler, P. Ye, K. S. Carslaw, J. Curtius, J. Dommen, J. Kirkby, M. Kulmala, I. Riipinen, D. R. Worsnop, N. M. Donahue and U. Baltensperger, The role of low-volatility organic compounds in initial particle growth in the atmosphere, *Nature*, 2016, **533**, 527–531.

14 C. Yan, W. Nie, A. L. Vogel, L. Dada, K. Lehtipalo, D. Stolzenburg, R. Wagner, M. P. Rissanen, M. Xiao, L. Ahonen, L. Fischer, C. Rose, F. Bianchi, H. Gordon, M. Simon, M. Heinritzi, O. Garmash, P. Roldin, A. Dias, P. Ye, V. Hofbauer, A. Amorim, P. S. Bauer, A. Bergen, A.-K. Bernhammer, M. Breitenlechner, S. Brilke, A. Buchholz, S. B. Mazon, M. R. Canagaratna, X. Chen, A. Ding, J. Dommen, D. C. Draper, J. Duplissy, C. Frege, C. Heyn, R. Guida, J. Hakala, L. Heikkinen, C. R. Hoyle, T. Jokinen, J. Kangasluoma, J. Kirkby, J. Kontkanen, A. Kürten, M. J. Lawler, H. Mai, S. Mathot, R. L. Mauldin, U. Molteni, L. Nichman, T. Nieminen, J. Nowak, A. Ojdanic, A. Onnela, A. Pajunoja, T. Petäjä, F. Piel, L. L. J. Quéléver, N. Sarnela, S. Schallhart, K. Sengupta, M. Sipilä, A. Tomé, J. Tröstl, O. Väisänen, A. C. Wagner, A. Ylisirniö, Q. Zha, U. Baltensperger, K. S. Carslaw, J. Curtius, R. C. Flagan, A. Hansel, I. Riipinen, J. N. Smith, A. Virtanen, P. M. Winkler, N. M. Donahue, V.-M. Kerminen, M. Kulmala, M. Ehn and D. R. Worsnop, Size-dependent influence of NO_x on the growth rates of organic aerosol particles, *Sci. Adv.*, 2020, **6**, eaay4945.

15 M. C. Jacobson, H.-C. Hansson, K. J. Noone and R. J. Charlson, Organic atmospheric aerosols: review and state of the science, *Rev. Geophys.*, 2000, **38**, 267–294.

16 M. Z. Jacobson, Global direct radiative forcing due to multicomponent anthropogenic and natural aerosols, *J. Geophys. Res.*, 2001, **106**, 1551–1568.

17 J. Merikanto, D. V. Spracklen, G. W. Mann, S. J. Pickering and K. S. Carslaw, Impact of nucleation on global CCN, *Atmos. Chem. Phys.*, 2009, **9**, 8601–8616.

18 I. Riipinen, J. R. Pierce, T. Yli-Juuti, T. Nieminen, S. Häkkinen, M. Ehn, H. Junninen, K. Lehtipalo, T. Petäjä, J. Slowik, R. Chang, N. C. Shantz, J. Abbatt, W. R. Leaitch, V.-M. Kerminen, D. R. Worsnop, S. N. Pandis, N. M. Donahue and M. Kulmala, Organic condensation: a vital link connecting aerosol formation to cloud condensation nuclei (CCN) concentrations, *Atmos. Chem. Phys.*, 2011, **11**, 3865–3878.

19 M. L. Luttkus, E. H. Hoffmann, A. Tilgner, R. Wolke, H. Herrmann and I. Tegen, Urban and Remote cheMistry modELLing with the new chemical mechanism URMELL: part I gas-phase mechanism development, *Environ. Sci.: Atmos.*, 2024, **4**, 164–189.

20 C. Knote, A. Hodzic and J. L. Jimenez, The effect of dry and wet deposition of condensable vapors on secondary organic aerosols concentrations over the continental US, *Atmos. Chem. Phys.*, 2015, **15**, 1–18.

21 M. F. Link, M. A. Pothier, M. P. Vermeuel, M. Riches, D. B. Millet and D. K. Farmer, In-Canopy Chemistry, Emissions, Deposition, and Surface Reactivity Compete to Drive Bidirectional Forest-Atmosphere Exchange of VOC Oxidation Products, *ACS ES&T Air*, 2024, **1**, 305–315.

22 J.-F. Müller, J. Peeters and T. Stavrakou, Fast photolysis of carbonyl nitrates from isoprene, *Atmos. Chem. Phys.*, 2014, **14**, 2497–2508.

23 N. L. Ng, S. S. Brown, A. T. Archibald, E. Atlas, R. C. Cohen, J. N. Crowley, D. A. Day, N. M. Donahue, J. L. Fry, H. Fuchs, R. J. Griffin, M. I. Guzman, H. Herrmann, A. Hodzic, Y. Iinuma, J. L. Jimenez, A. Kiendler-Scharr, B. H. Lee, D. J. Luecken, J. Mao, R. McLaren, A. Mutzel, H. D. Osthoff, B. Ouyang, B. Picquet-Varrault, U. Platt, H. O. T. Pye, Y. Rudich, R. H. Schwantes, M. Shiraiwa, J. Stutz, J. A. Thornton, A. Tilgner, B. J. Williams and R. A. Zaveri, Nitrate radicals and biogenic volatile organic compounds: oxidation, mechanisms, and organic aerosol, *Atmos. Chem. Phys.*, 2017, **17**, 2103–2162.

24 R. Suarez-Bertoa, B. Picquet-Varrault, W. Tamas, E. Pangui and J.-F. Doussin, Atmospheric Fate of a Series of Carbonyl Nitrates: Photolysis Frequencies and OH-Oxidation Rate Constants, *Environ. Sci. Technol.*, 2012, **46**, 12502–12509.

25 K. Tsigaridis, N. Daskalakis, M. Kanakidou, P. J. Adams, P. Artaxo, R. Bahadur, Y. Balkanski, S. E. Bauer, N. Bellouin, A. Benedetti, T. Bergman, T. K. Berntsen, J. P. Beukes, H. Bian, K. S. Carslaw, M. Chin, G. Curci, T. Diehl, R. C. Easter, S. J. Ghan, S. L. Gong, A. Hodzic, C. R. Hoyle, T. Iversen, S. Jathar, J. L. Jimenez, J. W. Kaiser, A. Kirkevåg, D. Koch, H. Kokkola, Y. H. Lee, G. Lin, X. Liu, G. Luo, X. Ma, G. W. Mann, N. Mihalopoulos, J.-J. Morcrette, J.-F. Müller, G. Myhre, S. Myriokefalitakis, N. L. Ng, D. O'Donnell, J. E. Penner, L. Pozzoli, K. J. Pringle, L. M. Russell, M. Schulz, J. Sciare, Ø. Seland, D. T. Shindell, S. Sillman, R. B. Skeie, D. Spracklen, T. Stavrakou, S. D. Steenrod, T. Takemura, P. Tiitta, S. Tilmes, H. Tost, T. Van Noije, P. G. Van Zyl, K. Von Salzen, F. Yu, Z. Wang, Z. Wang, R. A. Zaveri, H. Zhang, K. Zhang, Q. Zhang and X. Zhang, The AeroCom evaluation and intercomparison of organic aerosol in global models, *Atmos. Chem. Phys.*, 2014, **14**, 10845–10895.

26 R. Atkinson and J. Arey, Gas-phase tropospheric chemistry of biogenic volatile organic compounds: a review, *Atmos. Environ.*, 2003, **37**, 197–219.

27 M. Mahilang, M. K. Deb and S. Pervez, Biogenic secondary organic aerosols: a review on formation mechanism, analytical challenges and environmental impacts, *Chemosphere*, 2021, **262**, 127771.

28 M. L. Luttkus, E. H. Hoffmann, L. Poulain, A. Tilgner and R. Wolke, The Effect of Land Use Classification on the Gas-Phase and Particle Composition of the Troposphere: Tree Species Versus Forest Type Information, *J. Geophys. Res.: Atmos.*, 2022, **127**, e2021JD035305.

29 K. C. Barsanti, A. G. Carlton and S. H. Chung, Analyzing experimental data and model parameters: implications for predictions of SOA using chemical transport models, *Atmos. Chem. Phys.*, 2013, **13**, 12073–12088.

30 A. G. Carlton, P. V. Bhave, S. L. Napelenok, E. O. Edney, G. Sarwar, R. W. Pinder, G. A. Pouliot and M. Houyoux, Model Representation of Secondary Organic Aerosol in CMAQv4.7, *Environ. Sci. Technol.*, 2010, **44**, 8553–8560.

31 A. W. H. Chan, M. N. Chan, J. D. Surratt, P. S. Chhabra, C. L. Loza, J. D. Crounse, L. D. Yee, R. C. Flagan, P. O. Wennberg and J. H. Seinfeld, Role of aldehyde chemistry and NO_x concentrations in secondary organic aerosol formation, *Atmos. Chem. Phys.*, 2010, **10**, 7169–7188.

32 J. Dommen, A. Metzger, J. Duplissy, M. Kalberer, M. R. Alfarra, A. Gascho, E. Weingartner, A. S. H. Prevot, B. Verheggen and U. Baltensperger, Laboratory observation of oligomers in the aerosol from isoprene/NO_x photooxidation, *Geophys. Res. Lett.*, 2006, **33**, L13805.

33 J. H. Kroll, N. L. Ng, S. M. Murphy, R. C. Flagan and J. H. Seinfeld, Secondary organic aerosol formation from isoprene photooxidation under high-NO_x conditions, *Geophys. Res. Lett.*, 2005, **32**, L18808.

34 J. H. Kroll, N. L. Ng, S. M. Murphy, R. C. Flagan and J. H. Seinfeld, Secondary Organic Aerosol Formation from Isoprene Photooxidation, *Environ. Sci. Technol.*, 2006, **40**, 1869–1877.

35 S. M. Blichner, T. Yli-Juuti, T. Mielonen, C. Pöhlker, E. Holopainen, L. Heikkinen, C. Mohr, P. Artaxo, S. Carbone, B. B. Meller, C. Quaresma Dias-Júnior, M. Kulmala, T. Petäjä, C. E. Scott, C. Svenhag, L. Nieradzik, M. Sporre, D. G. Partridge, E. Tovazzi, A. Virtanen, H. Kokkola and I. Riipinen, Process-evaluation of forest aerosol-cloud-climate feedback shows clear evidence from observations and large uncertainty in models, *Nat. Commun.*, 2024, **15**, 969.

36 S. Gu, A. Guenther and C. Faiola, Effects of Anthropogenic and Biogenic Volatile Organic Compounds on Los Angeles Air Quality, *Environ. Sci. Technol.*, 2021, **55**, 12191–12201.

37 J. L. Jimenez, M. R. Canagaratna, N. M. Donahue, A. S. H. Prevot, Q. Zhang, J. H. Kroll, P. F. DeCarlo, J. D. Allan, H. Coe, N. L. Ng, A. C. Aiken, K. S. Docherty, I. M. Ulbrich, A. P. Grieshop, A. L. Robinson, J. Duplissy, J. D. Smith, K. R. Wilson, V. A. Lanz, C. Hueglin,

Y. L. Sun, J. Tian, A. Laaksonen, T. Raatikainen, J. Rautiainen, P. Vaattovaara, M. Ehn, M. Kulmala, J. M. Tomlinson, D. R. Collins, M. J. Cubison, E. J. Dunlea, J. A. Huffman, T. B. Onasch, M. R. Alfarra, P. I. Williams, K. Bower, Y. Kondo, J. Schneider, F. Drewnick, S. Borrmann, S. Weimer, K. Demerjian, D. Salcedo, L. Cottrell, R. Griffin, A. Takami, T. Miyoshi, S. Hatakeyama, A. Shimono, J. Y. Sun, Y. M. Zhang, K. Dzepina, J. R. Kimmel, D. Sueper, J. T. Jayne, S. C. Herndon, A. M. Trimborn, L. R. Williams, E. C. Wood, A. M. Middlebrook, C. E. Kolb, U. Baltensperger and D. R. Worsnop, Evolution of Organic Aerosols in the Atmosphere, *Science*, 2009, **326**, 1525–1529.

38 P. Forster, T. Storelvmo, K. Armour, W. Collins, J.-L. Dufresne, D. Frame, D. J. Lunt, T. Mauritsen, M. D. Palmer, M. Watanabe, M. Wild and H. Zhang, in *Climate Change 2021: The Physical Science Basis. Contribution of Working Group I to the Sixth Assessment Report of the Intergovernmental Panel on Climate Change*, ed. V. Masson-Delmotte, P. Zhai, A. Pirani, S. L. Connors, C. Péan, S. Berger, N. Caud, Y. Chen, L. Goldfarb, M. I. Gomis, M. Huang, K. Leitzell, E. Lonnoy, J. B. R. Matthews, T. K. Maycock, T. Waterfield, O. Yelekçi, R. Yu and B. Zhou, Cambridge University Press, Cambridge, United Kingdom and New York, NY, USA, 2023, ch. 7, pp. 923–1054.

39 P. Messina, J. Lathière, K. Sindelarova, N. Vuichard, C. Granier, J. Ghattas, A. Cozic and D. A. Hauglustaine, Global biogenic volatile organic compound emissions in the ORCHIDEE and MEGAN models and sensitivity to key parameters, *Atmos. Chem. Phys.*, 2016, **16**, 14169–14202.

40 G. Thornhill, W. Collins, D. Olivié, R. B. Skeie, A. Archibald, S. Bauer, R. Checa-Garcia, S. Fiedler, G. Folberth, A. Gjermundsen, L. Horowitz, J.-F. Lamarque, M. Michou, J. Mulcahy, P. Nabat, V. Naik, F. M. O'Connor, F. Paulot, M. Schulz, C. E. Scott, R. Séférian, C. Smith, T. Takemura, S. Tilmes, K. Tsigaridis and J. Weber, Climate-driven chemistry and aerosol feedbacks in CMIP6 Earth system models, *Atmos. Chem. Phys.*, 2021, **21**, 1105–1126.

41 L. Dada, D. Stolzenburg, M. Simon, L. Fischer, M. Heinritzi, M. Wang, M. Xiao, A. L. Vogel, L. Ahonen, A. Amorim, R. Baalbaki, A. Baccarini, U. Baltensperger, F. Bianchi, K. R. Daellenbach, J. DeVivo, A. Dias, J. Dommen, J. Duplissy, H. Finkenzeller, A. Hansel, X.-C. He, V. Hofbauer, C. R. Hoyle, J. Kangasluoma, C. Kim, A. Kürten, A. Kvashnin, R. Mauldin, V. Makhmutov, R. Marten, B. Mentler, W. Nie, T. Petäjä, L. L. J. Quéléver, H. Saathoff, C. Tauber, A. Tome, U. Molteni, R. Volkamer, R. Wagner, A. C. Wagner, D. Wimmer, P. M. Winkler, C. Yan, Q. Zha, M. Rissanen, H. Gordon, J. Curtius, D. R. Worsnop, K. Lehtipalo, N. M. Donahue, J. Kirkby, I. El Haddad and M. Kulmala, Role of sesquiterpenes in biogenic new particle formation, *Sci. Adv.*, 2023, **9**, eadi5297.

42 T. E. Lane, N. M. Donahue and S. N. Pandis, Simulating secondary organic aerosol formation using the volatility basis-set approach in a chemical transport model, *Atmos. Environ.*, 2008, **42**, 7439–7451.

43 T. Hoffmann, J. R. Odum, F. Bowman, D. Collins, D. Klockow, R. C. Flagan and J. H. Seinfeld, Formation of Organic Aerosols from the Oxidation of Biogenic Hydrocarbons, *J. Atmos. Chem.*, 1997, **26**, 189–222.

44 H. Li, M. R. Canagaratna, M. Riva, P. Rantala, Y. Zhang, S. Thomas, L. Heikkinen, P.-M. Flaud, E. Villenave, E. Perraudin, D. Worsnop, M. Kulmala, M. Ehn and F. Bianchi, Atmospheric organic vapors in two European pine forests measured by a Vocus PTR-TOF: insights into monoterpene and sesquiterpene oxidation processes, *Atmos. Chem. Phys.*, 2021, **21**, 4123–4147.

45 J. P. Nascimento, M. M. Bela, B. B. Meller, A. L. Banducci, L. V. Rizzo, A. L. Vara-Vela, H. M. J. Barbosa, H. Gomes, S. A. A. Rafee, M. A. Franco, S. Carbone, G. G. Cirino, R. A. F. Souza, S. A. McKeen and P. Artaxo, Aerosols from anthropogenic and biogenic sources and their interactions – modeling aerosol formation, optical properties, and impacts over the central Amazon basin, *Atmos. Chem. Phys.*, 2021, **21**, 6755–6779.

46 M. Shrivastava, M. O. Andreae, P. Artaxo, H. M. J. Barbosa, L. K. Berg, J. Brito, J. Ching, R. C. Easter, J. Fan, J. D. Fast, Z. Feng, J. D. Fuentes, M. Glasius, A. H. Goldstein, E. G. Alves, H. Gomes, D. Gu, A. Guenther, S. H. Jathar, S. Kim, Y. Liu, S. Lou, S. T. Martin, V. F. McNeill, A. Medeiros, S. S. de Sá, J. E. Shilling, S. R. Springston, R. A. F. Souza, J. A. Thornton, G. Isaacman-VanWertz, L. D. Yee, R. Ynoue, R. A. Zaveri, A. Zelenyuk and C. Zhao, Urban pollution greatly enhances formation of natural aerosols over the Amazon rainforest, *Nat. Commun.*, 2019, **10**, 1046.

47 R. Steinbrecher, G. Smiatek, R. Köble, G. Seufert, J. Theloke, K. Hauff, P. Ciccioli, R. Vautard and G. Curci, Intra- and inter-annual variability of VOC emissions from natural and semi-natural vegetation in Europe and neighbouring countries, *Atmos. Environ.*, 2009, **43**, 1380–1391.

48 R. Grote, M. Sharma, A. Ghirardo and J.-P. Schnitzler, A New Modeling Approach for Estimating Abiotic and Biotic Stress-Induced de novo Emissions of Biogenic Volatile Organic Compounds From Plants, *Front. For. Glob. Change*, 2019, **2**, 26.

49 A. C. Fitzky, H. Sandén, T. Karl, S. Fares, C. Calfapietra, R. Grote, A. Saunier and B. Rewald, The Interplay Between Ozone and Urban Vegetation—BVOC Emissions, Ozone Deposition, and Tree Ecophysiology, *Front. For. Glob. Change*, 2019, **2**, 50.

50 Ü. Niinemets, Mild versus severe stress and BVOCs: thresholds, priming and consequences, *Trends Plant Sci.*, 2010, **15**, 145–153.

51 Ü. Niinemets, A. Arneth, U. Kuhn, R. K. Monson, J. Peñuelas and M. Staudt, The emission factor of volatile isoprenoids: stress, acclimation, and developmental responses, *Biogeosciences*, 2010, **7**, 2203–2223.

52 J. D. Blande, J. K. Holopainen and Ü. Niinemets, Plant volatiles in polluted atmospheres: stress responses and

signal degradation: plant volatiles in a polluted atmosphere, *Plant, Cell Environ.*, 2014, **37**, 1892–1904.

53 R. Volkamer, J. L. Jimenez, F. San Martini, K. Dzepina, Q. Zhang, D. Salcedo, L. T. Molina, D. R. Worsnop and M. J. Molina, Secondary organic aerosol formation from anthropogenic air pollution: rapid and higher than expected, *Geophys. Res. Lett.*, 2006, **33**, 2006GL026899.

54 A. Hodzic, P. S. Kasibhatla, D. S. Jo, C. D. Cappa, J. L. Jimenez, S. Madronich and R. J. Park, Rethinking the global secondary organic aerosol (SOA) budget: stronger production, faster removal, shorter lifetime, *Atmos. Chem. Phys.*, 2016, **16**, 7917–7941.

55 W. R. Stockwell, F. Kirchner, M. Kuhn and S. Seefeld, A new mechanism for regional atmospheric chemistry modeling, *J. Geophys. Res.*, 1997, **102**, 25847–25879.

56 W. S. Goliff, W. R. Stockwell and C. V. Lawson, The regional atmospheric chemistry mechanism, version 2, *Atmos. Environ.*, 2013, **68**, 174–185.

57 M. G. Schultz, S. Stadtler, S. Schröder, D. Taraborrelli, B. Franco, J. Krefting, A. Henrot, S. Ferrachat, U. Lohmann, D. Neubauer, C. Siegenthaler-Le Drian, S. Wahl, H. Kokkola, T. Kühn, S. Rast, H. Schmidt, P. Stier, D. Kinnison, G. S. Tyndall, J. J. Orlando and C. Wespes, The chemistry–climate model ECHAM6.3-HAM2.3-MOZ1.0, *Geosci. Model Dev.*, 2018, **11**, 1695–1723.

58 L. K. Emmons, S. Walters, P. G. Hess, J.-F. Lamarque, G. G. Pfister, D. Fillmore, C. Granier, A. Guenther, D. Kinnison, T. Laepple, J. Orlando, X. Tie, G. Tyndall, C. Wiedinmyer, S. L. Baughcum and S. Kloster, Description and Evaluation of the Model for Ozone and Related Chemical Tracers, Version 4 (MOZART-4), *Geosci. Model Dev.*, 2010, **3**, 43–67.

59 G. Yarwood, Y. Shi and R. Beardsley, *Develop CB7 Chemical Mechanism for CAMx Ozone Modeling (Final Report Contract No. 582-19-90599)*, Ramboll US Corporation, Novato, CA, 2021.

60 W. P. L. Carter, Development of the SAPRC-07 chemical mechanism, *Atmos. Environ.*, 2010, **44**, 5324–5335.

61 W. P. L. Carter, *Documentation of the SAPRC-18 Mechanism (Report to California Air Resources Board Contract No. 11-761)*, College of Engineering, Center for Environmental Research and Technology, University of California, Riverside, CA, 2020.

62 T. Berndt, S. Richters, T. Jokinen, N. Hyttinen, T. Kurtén, R. V. Otkjær, H. G. Kjaergaard, F. Stratmann, H. Herrmann, M. Sipilä, M. Kulmala and M. Ehn, Hydroxyl radical-induced formation of highly oxidized organic compounds, *Nat. Commun.*, 2016, **7**, 13677.

63 A. Mutzel, Y. Zhang, O. Böge, M. Rodigast, A. Kolodziejczyk, X. Wang and H. Herrmann, Importance of secondary organic aerosol formation of α-pinene, limonene, and *m*-cresol comparing day- and nighttime radical chemistry, *Atmos. Chem. Phys.*, 2021, **21**, 8479–8498.

64 J. H. Seinfeld, G. B. Erdakos, W. E. Asher and J. F. Pankow, Modeling the Formation of Secondary Organic Aerosol (SOA). 2. The Predicted Effects of Relative Humidity on Aerosol Formation in the α-Pinene-, β-Pinene-, Sabinene-, Δ^3-Carene-, and Cyclohexene-Ozone Systems, *Environ. Sci. Technol.*, 2001, **35**, 1806–1817.

65 J. F. Pankow, J. H. Seinfeld, W. E. Asher and G. B. Erdakos, Modeling the Formation of Secondary Organic Aerosol. 1. Application of Theoretical Principles to Measurements Obtained in the α-Pinene/, β-Pinene/, Sabinene/, Δ^3-Carene/, and Cyclohexene/Ozone Systems, *Environ. Sci. Technol.*, 2001, **35**, 1164–1172.

66 D. Thomsen, J. Elm, B. Rosati, J. T. Skønager, M. Bilde and M. Glasius, Large Discrepancy in the Formation of Secondary Organic Aerosols from Structurally Similar Monoterpenes, *ACS Earth Space Chem.*, 2021, **5**, 632–644.

67 C. J. Colville and R. J. Griffin, The roles of individual oxidants in secondary organic aerosol formation from Δ^3-carene: 2. soa formation and oxidant contribution, *Atmos. Environ.*, 2004, **38**, 4013–4023.

68 B. Schell, I. J. Ackermann, H. Hass, F. S. Binkowski and A. Ebel, Modeling the formation of secondary organic aerosol within a comprehensive air quality model system, *J. Geophys. Res.*, 2001, **106**, 28275–28293.

69 H. O. T. Pye, A. W. H. Chan, M. P. Barkley and J. H. Seinfeld, Global modeling of organic aerosol: the importance of reactive nitrogen (NO_x and NO_3), *Atmos. Chem. Phys.*, 2010, **10**, 11261–11276.

70 B. N. Murphy and S. N. Pandis, Simulating the Formation of Semivolatile Primary and Secondary Organic Aerosol in a Regional Chemical Transport Model, *Environ. Sci. Technol.*, 2009, **43**, 4722–4728.

71 A. P. Tsimpidi, V. A. Karydis, M. Zavala, W. Lei, L. Molina, I. M. Ulbrich, J. L. Jimenez and S. N. Pandis, Evaluation of the volatility basis-set approach for the simulation of organic aerosol formation in the Mexico City metropolitan area, *Atmos. Chem. Phys.*, 2010, **10**, 525–546.

72 S. C. Farina, P. J. Adams and S. N. Pandis, Modeling global secondary organic aerosol formation and processing with the volatility basis set: implications for anthropogenic secondary organic aerosol, *J. Geophys. Res.*, 2010, **115**, D09202.

73 R. Ahmadov, S. A. McKeen, A. L. Robinson, R. Bahreini, A. M. Middlebrook, J. A. De Gouw, J. Meagher, E. -Y. Hsie, E. Edgerton, S. Shaw and M. Trainer, A volatility basis set model for summertime secondary organic aerosols over the eastern United States in 2006, *J. Geophys. Res.*, 2012, **117**, 2011JD016831.

74 J. Baek, Y. Hu, M. T. Odman and A. G. Russell, Modeling secondary organic aerosol in CMAQ using multigenerational oxidation of semi-volatile organic compounds, *J. Geophys. Res.*, 2011, **116**, D22204.

75 G. Hasan, R. R. Valiev, V.-T. Salo and T. Kurtén, Computational Investigation of the Formation of Peroxide (ROOR) Accretion Products in the OH- and NO_3-Initiated Oxidation of α-Pinene, *J. Phys. Chem. A*, 2021, **125**, 10632–10639.

76 G. Hasan, V.-T. Salo, T. Golin Almeida, R. R. Valiev and T. Kurtén, Computational Investigation of Substituent Effects on the Alcohol + Carbonyl Channel of Peroxy

Radical Self- and Cross-Reactions, *J. Phys. Chem. A*, 2023, **127**, 1686–1696.
77 O. Peräkylä, T. Berndt, L. Franzon, G. Hasan, M. Meder, R. R. Valiev, C. D. Daub, J. G. Varelas, F. M. Geiger, R. J. Thomson, M. Rissanen, T. Kurtén and M. Ehn, Large Gas-Phase Source of Esters and Other Accretion Products in the Atmosphere, *J. Am. Chem. Soc.*, 2023, **145**, 7780–7790.
78 T. Berndt, W. Scholz, B. Mentler, L. Fischer, H. Herrmann, M. Kulmala and A. Hansel, Accretion Product Formation from Self- and Cross-Reactions of RO2 Radicals in the Atmosphere, *Angew. Chem., Int. Ed.*, 2018, **57**, 3820–3824.
79 M. Ehn, J. A. Thornton, E. Kleist, M. Sipilä, H. Junninen, I. Pullinen, M. Springer, F. Rubach, R. Tillmann, B. Lee, F. Lopez-Hilfiker, S. Andres, I.-H. Acir, M. Rissanen, T. Jokinen, S. Schobesberger, J. Kangasluoma, J. Kontkanen, T. Nieminen, T. Kurtén, L. B. Nielsen, S. Jørgensen, H. G. Kjaergaard, M. Canagaratna, M. D. Maso, T. Berndt, T. Petäjä, A. Wahner, V.-M. Kerminen, M. Kulmala, D. R. Worsnop, J. Wildt and T. F. Mentel, A large source of low-volatility secondary organic aerosol, *Nature*, 2014, **506**, 476–479.
80 C. Mohr, F. D. Lopez-Hilfiker, T. Yli-Juuti, A. Heitto, A. Lutz, M. Hallquist, E. L. D'Ambro, M. P. Rissanen, L. Hao, S. Schobesberger, M. Kulmala, R. L. Mauldin III, U. Makkonen, M. Sipilä, T. Petäjä and J. A. Thornton, Ambient observations of dimers from terpene oxidation in the gas phase: implications for new particle formation and growth, *Geophys. Res. Lett.*, 2017, **44**, 2958–2966.
81 Y. Zhao, J. A. Thornton and H. O. T. Pye, Quantitative constraints on autoxidation and dimer formation from direct probing of monoterpene-derived peroxy radical chemistry, *Proc. Natl. Acad. Sci. U.S.A.*, 2018, **115**, 12142–12147.
82 M. Hallquist, J. C. Wenger, U. Baltensperger, Y. Rudich, D. Simpson, M. Claeys, J. Dommen, N. M. Donahue, C. George, A. H. Goldstein, J. F. Hamilton, H. Herrmann, T. Hoffmann, Y. Iinuma, M. Jang, M. E. Jenkin, J. L. Jimenez, A. Kiendler-Scharr, W. Maenhaut, G. McFiggans, T. F. Mentel, A. Monod, A. S. H. Prevot, J. H. Seinfeld, J. D. Surratt, R. Szmigielski and J. Wildt, The formation, properties and impact of secondary organic aerosol: current and emerging issues, *Atmos. Chem. Phys.*, 2009, **9**, 5155–5236.
83 B. Ervens, A. Sorooshian, Y. B. Lim and B. J. Turpin, Key parameters controlling OH-initiated formation of secondary organic aerosol in the aqueous phase (aqSOA), *J. Geophys. Res.: Atmos.*, 2014, **119**, 3997–4016.
84 B. Ervens, B. J. Turpin and R. J. Weber, Secondary organic aerosol formation in cloud droplets and aqueous particles (aqSOA): a review of laboratory, field and model studies, *Atmos. Chem. Phys.*, 2011, **11**, 11069–11102.
85 H. Herrmann, T. Schaefer, A. Tilgner, S. A. Styler, C. Weller, M. Teich and T. Otto, Tropospheric Aqueous-Phase Chemistry: Kinetics, Mechanisms, and Its Coupling to a Changing Gas Phase, *Chem. Rev.*, 2015, **115**, 4259–4334.
86 S. Stadtler, T. Kühn, S. Schröder, D. Taraborrelli, M. G. Schultz and H. Kokkola, Isoprene-derived secondary organic aerosol in the global aerosol–chemistry–climate model ECHAM6.3.0–HAM2.3–MOZ1.0, *Geosci. Model Dev.*, 2018, **11**, 3235–3260.
87 *GECKO-A*, **https://geckoa.lisa.u-pec.fr/index.php**, accessed May 2023.
88 S. Compernolle, K. Ceulemans and J.-F. Müller, EVAPORATION: a new vapour pressure estimation method for organic molecules including non-additivity and intramolecular interactions, *Atmos. Chem. Phys.*, 2011, **11**, 9431–9450.
89 *EVAPORATION*, **https://tropo.aeronomie.be/index.php/models/evaporation**, accessed May 2023.
90 D. Topping, M. Barley, M. K. Bane, N. Higham, B. Aumont, N. Dingle and G. McFiggans, UManSysProp v1.0: an online and open-source facility for molecular property prediction and atmospheric aerosol calculations, *Geosci. Model Dev.*, 2016, **9**, 899–914.
91 *UManSysProp*, **http://umansysprop.seaes.manchester.ac.uk**, accessed February 2022.
92 P. B. Myrdal and S. H. Yalkowsky, Estimating Pure Component Vapor Pressures of Complex Organic Molecules, *Ind. Eng. Chem. Res.*, 1997, **36**, 2494–2499.
93 R. C. Reid, J. M. Prausnitz and B. E. Poling, *The Properties of Gases and Liquids*, McGraw Hill Book Co., New York, NY, United States, 1987.
94 M. Camredon and B. Aumont, Assessment of vapor pressure estimation methods for secondary organic aerosol modeling, *Atmos. Environ.*, 2006, **40**, 2105–2116.
95 Y. Nannoolal, J. Rarey and D. Ramjugernath, Estimation of pure component properties: Part 3. Estimation of the vapor pressure of non-electrolyte organic compounds via group contributions and group interactions, *Fluid Phase Equilib.*, 2008, **269**, 117–133.
96 Y. Nannoolal, J. Rarey, D. Ramjugernath and W. Cordes, Estimation of pure component properties: Part 1. Estimation of the normal boiling point of non-electrolyte organic compounds via group contributions and group interactions, *Fluid Phase Equilib.*, 2004, **226**, 45–63.
97 R. Valorso, B. Aumont, M. Camredon, T. Raventos-Duran, C. Mouchel-Vallon, N. L. Ng, J. H. Seinfeld, J. Lee-Taylor and S. Madronich, Explicit modelling of SOA formation from α-pinene photooxidation: sensitivity to vapour pressure estimation, *Atmos. Chem. Phys.*, 2011, **11**, 6895–6910.
98 J. F. Pankow and W. E. Asher, SIMPOL.1: a simple group contribution method for predicting vapor pressures and enthalpies of vaporization of multifunctional organic compounds, *Atmos. Chem. Phys.*, 2008, **8**, 2773–2796.
99 M. A. H. Khan, M. E. Jenkin, A. Foulds, R. G. Derwent, C. J. Percival and D. E. Shallcross, A modeling study of secondary organic aerosol formation from sesquiterpenes using the STOCHEM global chemistry and transport model, *J. Geophys. Res.: Atmos.*, 2017, **122**, 4426–4439.
100 P. Middleton, W. R. Stockwell and W. P. L. Carter, Aggregation and analysis of volatile organic compound emissions for regional modeling, *Atmos. Environ., Part A*, 1990, **24**, 1107–1133.

101 R. Wolke, O. Knoth, O. Hellmuth, W. Schröder and E. Renner, in *Parallel Computing*, ed. G. R. Joubert, W. E. Nagel, F. J. Peters and W. V. Walter, North-Holland, 2004, vol. 13, pp. 363–369.

102 R. Wolke, W. Schröder, R. Schrödner and E. Renner, Influence of grid resolution and meteorological forcing on simulated European air quality: a sensitivity study with the modeling system COSMO–MUSCAT, *Atmos. Environ.*, 2012, **53**, 110–130.

103 M. Karl, H.-P. Dorn, F. Holland, R. Koppmann, D. Poppe, L. Rupp, A. Schaub and A. Wahner, Product study of the reaction of OH radicals with isoprene in the atmosphere simulation chamber SAPHIR, *J. Atmos. Chem.*, 2006, **55**, 167–187.

104 J. Lee-Taylor, A. Hodzic, S. Madronich, B. Aumont, M. Camredon and R. Valorso, Multiday production of condensing organic aerosol mass in urban and forest outflow, *Atmos. Chem. Phys.*, 2015, **15**, 595–615.

105 K. Sato, F. Ikemori, S. Ramasamy, A. Fushimi, K. Kumagai, A. Iijima and Y. Morino, Four- and Five-Carbon Dicarboxylic Acids Present in Secondary Organic Aerosol Produced from Anthropogenic and Biogenic Volatile Organic Compounds, *Atmosphere*, 2021, **12**, 1703.

106 J. M. Rosenfeld and C. B. Murphy, Hydrolysis study of organic acid anhydrides by differential thermal analysis—II: Maleic anhydride and trimellitic anhydride, *Talanta*, 1967, **14**, 91–96.

107 B. J. Dennis-Smither, F. H. Marshall, R. E. H. Miles, T. C. Preston and J. P. Reid, Volatility and Oxidative Aging of Aqueous Maleic Acid Aerosol Droplets and the Dependence on Relative Humidity, *J. Phys. Chem. A*, 2014, **118**, 5680–5691.

108 T. B. Nguyen, K. H. Bates, J. D. Crounse, R. H. Schwantes, X. Zhang, H. G. Kjaergaard, J. D. Surratt, P. Lin, A. Laskin, J. H. Seinfeld and P. O. Wennberg, Mechanism of the hydroxyl radical oxidation of methacryloyl peroxynitrate (MPAN) and its pathway toward secondary organic aerosol formation in the atmosphere, *Phys. Chem. Chem. Phys.*, 2015, **17**, 17914–17926.

109 H. G. Kjaergaard, H. C. Knap, K. B. Ørnsø, S. Jørgensen, J. D. Crounse, F. Paulot and P. O. Wennberg, Atmospheric Fate of Methacrolein. 2. Formation of Lactone and Implications for Organic Aerosol Production, *J. Phys. Chem. A*, 2012, **116**, 5763–5768.

110 E. Freney, K. Sellegri, M. Chrit, K. Adachi, J. Brito, A. Waked, A. Borbon, A. Colomb, R. Dupuy, J.-M. Pichon, L. Bouvier, C. Delon, C. Jambert, P. Durand, T. Bourianne, C. Gaimoz, S. Triquet, A. Féron, M. Beekmann, F. Dulac and K. Sartelet, Aerosol composition and the contribution of SOA formation over Mediterranean forests, *Atmos. Chem. Phys.*, 2018, **18**, 7041–7056.

111 G. Cirino, J. Brito, H. M. J. Barbosa, L. V. Rizzo, P. Tunved, S. S. de Sá, J. L. Jimenez, B. B. Palm, S. Carbone, J. V. Lavric, R. A. F. Souza, S. Wolff, D. Walter, J. Tota, M. B. L. Oliveira, S. T. Martin and P. Artaxo, Observations of Manaus urban plume evolution and interaction with biogenic emissions in GoAmazon 2014/5, *Atmos. Environ.*, 2018, **191**, 513–524.